Nucleic Acids Research, 2025, **53**, gkaf116
https://doi.org/10.1093/nar/gkaf116
Nucleic Acid Therapeutics

Virus-derived siRNA: Coronavirus and influenza virus trigger antiviral RNAi immunity in birds

Yaotang Wu[1], Peng Liu[2], Jie Zhou[1], Mei Fu[1], Chenlu Wang[3], Ningna Xiong[1], Wenxin Ji[1], Zhisheng Wang[4], Jian Lin[1,*], Qian Yang[1]

[1]College of Veterinary Medicine, Nanjing Agricultural University, Wei gang 1, Nanjing, Jiangsu 210095, PR China
[2]College of Veterinary Medicine, Jiangsu Agri-Animal Husbandry Vocational College, Taizhou, Jiangsu 225300, PR China
[3]College of Life Sciences, Nanjing Agricultural University, Wei gang 1, Nanjing, Jiangsu 210095, PR China
[4]Institute of Veterinary Immunology and Engineering, Jiangsu Academy of Agricultural Sciences, Nanjing 210014, PR China
[*]To whom correspondence should be addressed. Tel: +86 025 84395817; Fax: +86 025 84398669; Email: linjian@njau.edu.cn

Abstract

RNA interference (RNAi) is a key antiviral immune mechanism in eukaryotes. However, antiviral RNAi in vertebrates has only been observed in cells with poor interferon systems or in viral suppressors of RNAi (VSR) deficiency virus infections. Our research discovered that infecting macrophages with wild-type coronavirus (Infectious bronchitis virus, IBV) and influenza viruses (Avian influenza virus, AIV) can trigger RNAi antiviral immunity and produce a certain amount of virus-derived siRNA (vsiRNA). These vsiRNAs have an inhibitory effect on the virus and carry out targeted silencing along the Dicer-Ago2-vsiRNA axis. Notably, these vsiRNAs are distributed throughout the virus's entire genome, with a predilection for A/U at the 5′ and 3′ termini of vsiRNA. In addition, Dicer cleavage produces vsiRNA based on the RWM motif, where R represents A/G, W represents A/C, and M represents A/U. We also discovered that avian LGP2 and MDA5 proteins positively impact the expression of the Dicer protein and the Dicer subtype "DicerM." Most importantly, the PS-vsiRNA plasmid combined with nanomaterial polyetherimide (PEI) showed excellent anti-virus activity in specific-pathogen-free (SPF) chickens. These findings show that RNA viruses trigger the production of the vsiRNA in avian somatic cells, which is of great significance for the application of therapeutic vaccines.

Graphical abstract

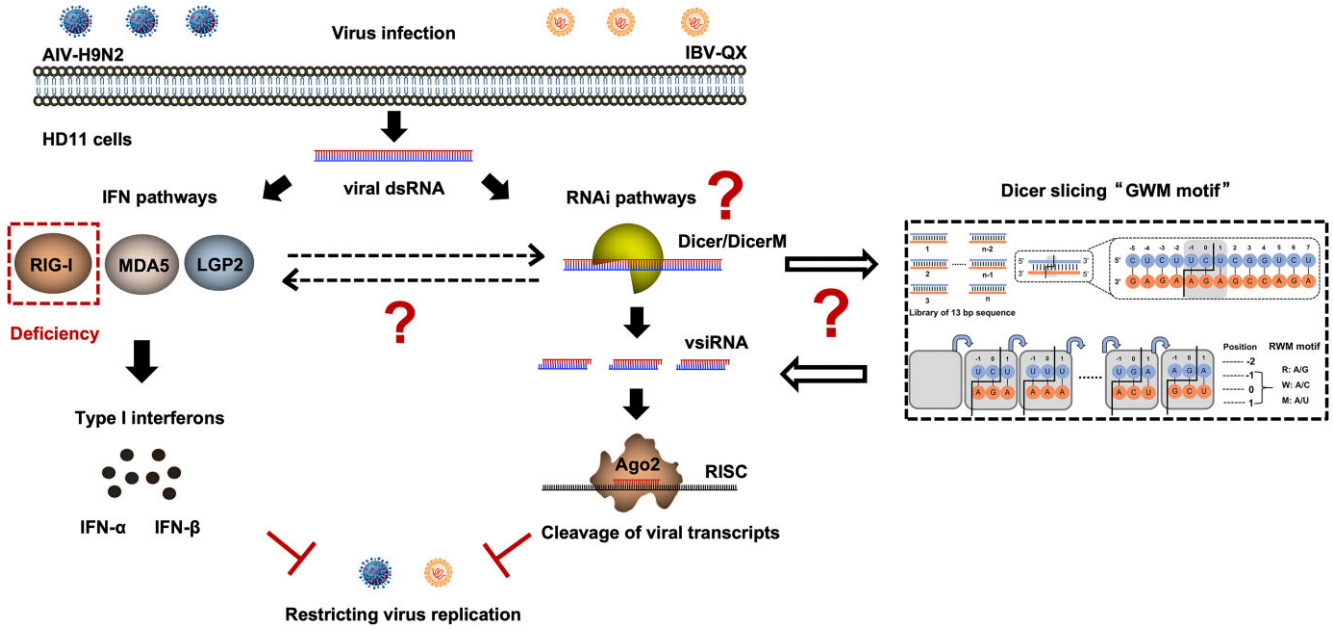

Received: September 30, 2024. **Revised:** January 30, 2025. **Editorial Decision:** January 31, 2025. **Accepted:** February 5, 2025

Introduction

RNA viruses have emerged as a significant threat to global health, with frequent outbreaks and challenges in containing their spread [1–3]. Influenza viruses and coronavirus are notoriously difficult to prevent and manage with conventional methods due to their high rate of mutation and capacity to adapt to new hosts and surroundings [4–6]. Elucidating the mechanisms of RNA virus infection and cell-defining strategies can lead to the identification of new targets for antiviral drugs and vaccines, as well as insights into how the immune system responds to these viruses [7].

The continuous conflict between viruses and their hosts is an amazing sight in virology, underscoring the complex dance of evolution. Two pivotal players in this drama are the interferon (IFN) and RNA interference (RNAi) pathways, which are fundamental antiviral defense mechanisms in hosts [8, 9]. The IFN pathway, characterized by its rapid response, is recognized for limiting viral spread, while the RNAi pathway, known for its precision, targets viral RNA specifically [10, 11]. However, the interplay between these pathways and their effectiveness against different types of RNA viruses remains a subject of intense study. As the avian antiviral system transitions from RNAi to IFN, it becomes more susceptible to RNA virus infections, including avian influenza virus (AIV) and chicken infectious bronchitis virus (IBV) [12, 13]. For these reasons, we selected the avian model to elucidate the interaction between RNAi and RNA viruses.

RNAi is involved in specific recognition and cleavage of viral dsRNAs, thereby preventing virus replication [14–16]. The core of RNAi lies in the production of small RNA molecules, which are generated in a sequence-specific manner and target only the complementary viral RNAs [17, 18]. To clarify the molecular mechanism of antiviral RNAi systems in birds, our study focused on three basic questions. (1) Can viral dsRNA be cleaved into virus-derived siRNA (vsiRNA)? (2) What is the mechanism by which vsiRNA exerts antiviral effects? (3) How to use the vsiRNA-based discovery in clinical settings? Although several studies have shown that mammals can harness RNAi against the Human enterovirus 71, Zika virus, and other RNA viruses in pluripotent or multipotent cells, these are associated with cells that exhibit low responsiveness to IFN [19–21]. Given that the avian IFN system lacks RIG-I receptors and several ISG genes, we selected the avian model to investigate the molecular interactions between RNAi and other key proteins in the RNA recognition pathway, such as LGP2 and MDA5, which differ from those observed in mammals [13]. This distinction could account for birds' stronger RNAi defenses against viral infections.

Finally, our study provides valuable insights into the antiviral mechanisms of the IFN and RNAi pathways, the discovery of a novel Dicer isoform "DicerM" in birds, and the potential application of vsiRNA in antiviral therapy. This research not only enhances our understanding of host-virus interactions but also lays the foundation for the development of novel antiviral strategies.

Materials and methods

Animals, viruses, and cells

The 2-week-old Specific-Pathogen-Free (SPF) white leghorn chickens were purchased by Nanjing Te Awesome Planting Professional Cooperative (Nanjing, China). IBV strain QX ($EID_{50} = 10^{-5.8}$/0.1 mL), IBDV BC6/85 strain ($TCID_{50} = 10^{-4.5}$/0.1 mL), and AIV strain H9N2 ($EID_{50} = 10^{-7}$/0.1 mL) were kindly provided by the Jiangsu Academy of Agricultural Sciences (JAAS, Nanjing, China) and stored in our lab. The medium was switched to RPMI 1640 or Dulbecco's modified Eagle's medium (DMEM) containing 2% fetal bovine serum (FBS) without antibiotics before virus inoculation. Biosafety Level 2 (BSL-2) labs were used for virus infection experiments in the mucosal immunology group.

HD11 cells, DF-1 cells, Chicken liver cancer cells (LMH), 293T cells and Madin-Darby Canine Kidney cells (MDCK) were commercially obtained from American Type Culture Collection (ATCC) and maintained in RPMI 1640 or DMEM supplemented with 10% FBS, penicillin (100 U/ml), and streptomycin (100 mg/mL) at 37°C in a humidified atmosphere with 5% CO2. PBMCs-Mφ were isolated from peripheral blood mononuclear cells (PBMCs) of specific-pathogen-free (SPF) chickens by using Histopaque-1077 (Sigma-Aldrich) and kept in -80°C. Dicer knockout ($Dicer^{-/-}$) HD11 cells line and Ago2 knockout ($Ago2^{-/-}$) HD11 cells line were constructed via CRISPR/Cas9 system. This study was approved by the Ethics Committee of the Animal Experiments Center, and the Institutional Animal Care and Use Committee of Nanjing Agricultural University, and was carried out by the National Institutes of Health guidelines.

Viruses infection

In cell experiments, regarding the pertinent literature concerning the MOI of macrophages infected with IBV and AIV, our manuscript specifies the following infection levels: IBV-QX at an MOI of 5, AIV-H9N2 at an MOI of 1, and IBDV at an MOI of 0.1, respectively [22–24]. They were incubated at 37°C with 5% CO_2 for 2 h and then cleaned using RPMI 1640 or DMEM. The non-infected virus cells for the Blank group. The Mock group represents adding only RPMI-1640 medium to cells and infecting them with the corresponding virus as a positive control in the experiment. The RNA and protein samples were collected according to the indicated time (24 and 48 h). For animal experiments, the different experimental group was inoculated with $10^4 EID_{50}$ of AIV-H9N2 or IBDV. On the the fourth day after infection, the lungs and bursa of Fabricius were collected for histological section and hematoxylin-eosin (HE) staining.

RNA extraction, reverse transcription, PCR and qRT-PCR

Total RNAs from cells were extracted with the TRIzol™ reagent (Invitrogen) according to the manufacturer's instructions. Around 500 ng/μL RNA was reverse transcribed to cDNA by using HiScript II Q Select RT SuperMix for qPCR (Vazyme) according to the manufacturer's instructions. For PCR experiments, cDNA was amplified in 35 cycles of PCR using Dicer and DicerM-specific primers, the β-actin as control. For qRT-PCR data, the ChamQ Universal SYBR qPCR Master Mix (Vazyme) was used in the application 7500 fast real-time PCR system (Thermofisher). The gene expression levels were normalized to gallus β-actin or gallus GAPDH. Compare with the Control group in terms of statistics to obtain $2^{-\Delta\Delta Ct}$, and the final result is that the Control group is "1" and the virus-infected group or other experimental group is different multiples of the Control group. All the primers were designed and produced by Sangon Biotech Co., Ltd.

(Shanghai, China). The detailed information on all primers is listed in Supplementary Table S1.

Western blotting assay

Around 100 μL RIPA-PMSF lysates from cultured cells were determined concentration through Bicinchonic Acid Assay and were resolved on SDS-PAGE, semidry transferred onto a polyvinylidene fluoride membrane (PVDF), and stained at 4°C overnight with mouse anti-β-actin (1:5000), rabbit anti-GAPDH (1:5000), rabbit anti-Dicer (1:500), rabbit anti-Ago2 (1:500), rabbit anti-LGP2 (1:500), rabbit anti-MDA5 (1:500), mouse anti-GFP (1:10 000), mouse anti-his (1:2000), mouse anti-myc (1:1 000), mouse anti-IBV N (1: 5000), and mouse anti-IBDV VP2 (1:100). The signal was developed using Goat anti-Rabbit/Mouse IgG(H&L)-HRP secondary antibody (1:5 000) and multifunctional gel image analysis system (Tanon, China) by using Ultrasensitive ECL chemiluminescence Kit.

CO-immunoprecipitation assay

The recombinant plasmids PC-Dicer, PC-DicerM, PC-LGP2, and PC-MDA5 were co-transfected into 293T cells in a 1:1 ratio. After 24 h, the culture medium was discarded and washed three times with PBS. The cells were collected in centrifuge tubes and IP Lysis/Wash Buffer containing PMSF was added. After mixing, they were placed on ice for 20 min and mixed several times to fully lyse the cells and release the protein. Collect cell samples according to CO-immunoprecipitation (Co-IP) Kit (YEASEN) and perform the following operations: (1) take 25 μL of Anti-myc/his magnetic beads and IgG antibody magnetic Beads separately into clean centrifuge tubes; (2) add pre-cooled PBS to the magnetic beads, gently mix and collect the discarded supernatant using a magnetic rack; (3) add 200 μL of IP Lysis/Wash Buffer to the centrifuge tube. Gently mix with a pipette for 1 min, collect the magnetic beads with a magnetic rack, and discard the supernatant; (4) add the prepared protein sample containing myc/his labeling into a centrifuge tube containing magnetic beads and maintain mixing incubate overnight at 4°C in a uniform state; (5) collect magnetic beads using a magnetic rack and remove unbound samples; (6) add 200 μL of IP lysis/wash buffer to the centrifuge tube and gently mix with a pipette. Collecting magnetism, discard the supernatant and repeat twice; (7) add 100 μL Elution Buffer to the centrifuge tube for elution, keep it mixed and incubate at room temperature for 10 min, then add 10 μL neutralization buffer to neutralize the low pH. Separate magnetic beads using a magnetic stand and retain the supernatant containing the target antigen for western blotting validation.

Deep sequencing and bioinformatic analysis of small RNAs

After 24 h of infection with 1 MOI AIV-H9N2 and 5 MOI IBV-QX in HD11 cells, RNA samples were extracted using the TRIzol method and subjected to RNA deep sequencing. The sequencing method and data analysis were as described previously [11, 25, 26]. Libraries of small RNAs cloned from cultured gallus cells were sequenced by an Illumina HiSeq 2000/2500 at the Hangzhou Lianchuan Biotechnology Co., Ltd. Small RNA reads were mapped to the virus and host genome references or compared to mature miRNAs. Mapping was done by ACGT101-miR (v4.2) and Bowtie 1.0.0 with either a perfect match or two mismatches [5]. All reference sequences were downloaded from the NCBI website, as listed below. Gallus genome bGalGal1 for the NCBI RefSeq (GenBank: GCA-016699485.1), AIV-H9N2 for the (GenBank: KP865772.1), and IBV-QX for the (GenBank: ON260865.1). Notely, the adapter sequence for the sequencing is 5′Adaptor (5ADT): GTTCAGAGTTCTACAGTCCGACGATC, and the 3′Adaptor (3ADT): TGGAATTCTCGGGTGCCAAGG. Pairs of complementary 21 nt vsiRNA or other high-abundance vsiRNA in each library with different base-pairing lengths were computed using a previously described algorithm10, which calculates the total counts of pairs in each nucleotide distance between the 5′ and 3′ ends of complementary 21 nt vsiRNA or corresponding vsiRNA. The following of *Yang Li. et al*. equations were used to do the correlation analysis of small RNA populations [25].

Other group vsiRNA data analysis

To start, use the Gene Expression Omnibus (GEO) on the NCBI website to query data by entering keywords. Download the compressed GEO Series (GSE) package for the relevant group (GSE147658, GSE11868, GSE90095, GSE61251, GSE151033, GSE213638, GSE162317, and GSE193555). For the AIV group are the Influenza A virus (A/chicken/Jiangsu/A2093/2011(H9N2)) and the GenBank number as follow, KP865892.1, KP865845.1, KP865799.1, KP865958.1, KP866002.1, KP866046.1, and KP866088.1. For the NDV group are the F48E9 (GenBank: MG456905.1) and LaSota (GenBank: MG456905.1), and the IBDV group is divided into A chain (GenBank: MZ740264.1) and B chain (GenBank: MZ740265.1). Besides, the BVDV, BRSV, and BTV groups need to be aligned and filtered the Bos taurus NCBI RefSeq (GenBank: GCA-002263795.4) and Ovis aries (GenBank: GCA-016772045.2). Meanwhile, the virus reference sequences are as follows, BVDV (GenBank: NC_001461.1), BRSV (GenBank: MG947594.1), and BTV (GenBank: KC879615.1, KC879616.1, KC879613.1, KC879619.1, KC879620.1, KC879621.1, KC879621.1, KC879623.1, and KC879624.1). The SARS-CoV-2 group was divided into three types of infected-cells, A549-ACE2 cells, Caco-2, and human small airway epithelial cells (SAECs). Comparatively, SARS-CoV-2 group vsiRNA analysis needs to align the BetaCoV/Wuhan/IPBCAMS-WH-04/2019 strain (GeneBank: MT019532.1) and SARS-CoV-2 USA-WA1/2020 strain (GeneBank: MT246667.1).

Submit the collected GSE dataset, host genome, and corresponding viral nucleic acid sequences (FASTA format) to Mormer Biotechnology Co., Ltd. (Nanjing, China) for bioinformatics analysis. The data returned by sample sequencing is generally stored in a fastq file, usually in a compressed file format of filename.fq.gz. Firstly, count the reads of small RNA sequencing and convert U into T, and then compare them with the host genome to filter the siRNAs that match the host genome. Compare the siRNAs that do not match the host genome with the virus genome, screen the siRNAs that match the virus, and count the number of siRNA with a length of 18–25 nt (especially 21–23 nt).

Plasmids and vsiRNA details

Construction of the overexpression plasmid. For the PC-DicerM construction, DicerM cDNA was amplified using PCR and introduced into the *Hin*d III and 6 × His tagged-*Xho*I site, cut and inserted into the pcDNA3.1-EGFP-C

(YouBio, China) to generated C-term 6 × His tagged DicerM fusion by use T4 DNA ligase (ATG Biotechnology, Nanjing, China). Regarding the PC-Dicer and PC-Ago2, we used the pcDNA3.1/myc-His B (+) vector (YouBio) as the skeleton carrier, to produce C-term myc-tagged Dicer and Ago2 fusion. Besides, the construction method of the plasmid PC-LGP2 and PC-MDA5 are consistent with PC-Dicer. For the silenced plasmids (PS-Dicer, PS-DicerM, PS-LGP2, and PS-MDA5) were constructed and saved by our lab are listed in Supplementary Table S4. In the PS-vsiRNA plasmid construction, vsiRNA was chosen by the vsiRNA enrichment zone (M, NS1, VP5, and VP3) and cloned into the skeleton vector pSilencer4.1 (PS) through homologous recombination, followed by the shRNA plasmid construction protocol [27]. The PC-vsiRNA-EGFP and PC-NC-EGFP plasmid were synthesized using Youbio company's chemical method, which was the insert fragment we selected. All the plasmids were preserved in our lab. The control plasmid groups were the pcDNA3.1-EGFP-C, pcDNA3.1(+)/myc-His B (PC), and the psilencer4.1-CMV-neo (PS). The PC is an eukaryotic expression plasmid that can efficiently express the target protein, while PS-siRNA and PS-vsiRNA plasmids can express a large number of siRNA fragments. For the next LGP2 and MDA5 experiments, I adjusted the amount of transfection reagent to 3 μL and the amount of plasmid to 2 μg, dissolved them in the 1640 medium and allowed them to stand for 5 min. After mixing, they were allowed to stand for another 5 min before being added to the cells.

Double-stranded vsiRNA and the oligo transfection test

The double-stranded vsiRNA used in this study was prepared by *in vitro* T7 transcription. The templates for RNA synthesis were generated by PCR amplification. The sequences of the double-stranded vsiRNA and oligos are shown in Supplementary Table S3. Cells were seeded at 80% confluency in six-well plates and transfected with 200 nM double-stranded vsiRNA and single oligo with lipofectamine 3000 as described above. HD11 cells were transfected with the AIV-vsiRNA oligo (+), AIV-vsiRNA oligo (-), and AIV double-stranded vsiRNA (200 nM) for 12 h, then infected the 1 MOI AIV-H9N2 and subjected to western blotting to detect the AIV-NP expression for 24 h. It should be noted that the sequence of vsiRNA shown in Supplementary Table S3 of this manuscript, which is completely identical to the virus sequence, is represented as vsiRNA (+), while vsiRNA (-) is represented as a sequence that is completely complementary to vsiRNA (+) and is not shown in Supplementary Table S3.

Fluorescence attenuation test

Cloned the 90 bp virus sequence containing the high abundance vsiRNA targeting region into the pcDNA3.1-EGFP vector, to produce the pcDNA3.1-vsiRNA-EGFP plasmid (PC-vsiRNA-EGFP) and not contain vsiRNA region as the control group pcDNA3.1-NC-EGFP (PC-NC-EGFP). After transfection of PC-vsiRNA-EGFP plasmid in the indicate HD11 cells (WT, Dicer $^{-/-}$, and Ago2 $^{-/-}$) for 12 h, infection was performed with 1 MOI AIV-H9N2, and green fluorescence observation was performed 24 h after infection. Fluorescent images were presented under a confocal laser microscope (Zeiss, Germany). As for the replenishment test, the fluorescence attenuation test mentioned above should be performed after the transfection of PC-Dicer, the PC-Ago2, and the PC-vsiRNA-EGFP into knockout cells for 24 h.

PS-vsiRNA and PPvPNs protection test

The PS-VP5-VP3 protection experiment is divided into cell and SPF chicken part. The psilencer 4.1-CMV-neo (PS) plasmid and PS-VP5-VP3 were transfected into a 6-well plate for 24 h and then infected with 10^3EID$_{50}$ IBDV for the qRT-PCR, western blotting and plaque test. Lastly, SPF chickens were immunized with PS-VP5-VP3 plasmid and PEI at an NP ratio of 6.5 (nitrogen and phosphorus) for 24 h and then challenged with 10^3EID$_{50}$ IBDV. The bursa of Fabricius was collected for the HE staining to determine the protective effect of PS-VP3. Besides, the steps of using PS-M-NS1 plasmid for AIV-H9N2 antiviral test are similar to those of the IBDV group test.

CRISPR-Cas9 knockout and siRNA/PS-shRNA knockdown

Dicer and Ago2 knockout (KO) clones were generated by transfection of HD11 cells with Cas9-Dicer sgRNA pX459 (Cas9-Dicer) and Cas9-Ago2 sgRNA pX459 (Cas9-Ago2), selection under 4 μg/mL puromycin (Sangon Biotech) for 3 days, and single-cell cloning as described previously [28]. The resulting clones were confirmed by sequencing and western blotting. The online tool from the Zhang Feng laboratory (http://crispr.mit.edu/) was used to design Dicer and Ago2 guide RNAs. Dicer sgRNA was used TCGAACTGCTGCCGTTCATATGG with the Dicer sgRNA-F primer (5′-CACCGTCGAACTGCTGCCGTTCATA-3′) and Dicer sgRNA-R primer (5′-AAACTATGAACG-GCAGCAGTTCGAC-3′). Ago2 sgRNA was used GCTTTATATCCAACTCGTAATGG with the Ago2 sgRNA-F primer (5′-CACCGCTTTATATCCAACTCGTAA-3′) and Ago2 sgRNA primer (5′-AAACTTACGAGTTGGATATAAAGC-3′). Cells surviving puromycin selection were seeded in single-cell dilutions in 96-well plates, cultured, and expanded into fasks. The Dicer and Ago2 knockout were validated by Sanger sequencing and western blotting. HD11 cells were transfected with the siRNA, PS-Dicer, PS-Ago2, PS-MDA5, and PS-LGP2, subjected to qRT-PCR and western blotting to detect the gene expression for 24 and 48 h.

Plaque assays

For the IBDV test. After 2 h of infection, discard the virus solution and wash with DMEM three times, pour the agar mixture (2% low melting point agar, 5% Excell serum, 2 × DMEM) into the well, and continue to culture at 37°C for 3 days. After being fixed with 4% paraformaldehyde for 2 h, crystal violet staining was performed, and the antiviral effect was determined by the number and size of the plaque.

For the AIV test, there is a slight difference in the plaque test between the AIV group and the IBDV group. Transfer the cell supernatant of HD11 cells infected with AIV to MDCK cells after 24 h. Plaque assays were performed on MDCK cells in 6-well plates and were incubated at 37°C for 2 h to allow adsorption.

The docking analysis

The docking steps for Dicer, DicerM, LGP2, and MDA5 molecules are as follows. Protein pretreatment: Download

protein structures from the PDB database, use Pymol to remove protein solvent molecules and impurities, hydrogenate and calculate charges. Ligand pretreatment: Download small molecule structures, preprocess small molecules using Autodock, hydrogenate and calculate charges. Defining active sites, the selection of active sites is usually based on the structural information and relevant biological activity data of proteins. The active site is not exactly equal to the receptor binding site, but in most cases they overlap with each other. Determine a reasonable search space based on the active site and limit the exploration range of ligands to improve computational efficiency. Use appropriate molecular docking algorithms to quickly explore multiple ligand conformations in the search space and evaluate their binding energies with proteins. Analyze the docking results, including predicting the optimal ligand conformation, binding site, and interaction mode. Use a scoring function to evaluate different conformations and determine their affinity and stability. Based on the docking results, subsequent structural optimization can be carried out, including introducing modifying groups, designing drug derivatives, etc., to further improve binding affinity and selectivity.

Hematoxylin-eosin staining of the bursa of Fabricius and lung

The fixed paraffin sections of the bursa of Fabricius were cut into 5 μm sections. Remove the paraffin from the slices with xylene, then pass through high to low-concentration alcohol, and finally add distilled water to stain. Hematoxylin (H) is an alkaline dye, which can dye the nucleus and cell kernel sugar body into blue-purple. The structure dyed by the alkaline dye is basophilic. Eosin (E) is an acidic dye that can dye the cytoplasm red or light red.

Statistical analyses

Quantitative and statistical analyses of data were performed using GraphPad Prism 8.3.0. One-way analysis of variance (ANOVA) was used to determine significant differences among multiple groups, while t-tests were employed to identify differences between two groups. Error bars representing the standard deviation (SD) were utilized to present the corresponding legends. Statistical significance in the figures was indicated as: $****P < 0.0001$, $***P < 0.001$, $**P < 0.01$, $*P < 0.05$; ns, insignificant. Data were combined from at least three independent experiments unless otherwise stated. All used resources and reagents are listed in Supplementary Table S2.

Results

AIV and IBV infection triggers the production of vsiRNA in macrophages

IFN and RNAi are two crucial antiviral mechanisms, and their expression can illustrate the relationship between host antiviral resistance and viral immune evasion. When we infected macrophages (HD11 cells) with two respiratory viruses (AIV and IBV) in birds, the mRNA expression levels of key genes involved in the IFN pathway, such as MDA5, TLR3, IFN-α, IFN-β, TLR7, IFN-γ, and MyD88, exhibited significant increases (Fig. 1A and B and Supplementary Fig. S1A and B). However, the qRT-PCR results demonstrated a significant increase in the viral load of AIV-H9N2 and IBV-QX in macrophages, indicating that the rapid response of the IFN pathway does not effectively limit the viral load in macrophages following RNA virus infection (Fig. 1A and B). Besides, western blotting results indicated that AIV-H9N2 and IBV-QX infections lead to a significant decrease in the core proteins Dicer and Ago2 within the RNAi pathway (Fig. 1C and D). This suggests that RNA viruses (AIV and IBV) may facilitate their replication by inhibiting the RNAi pathway.

The way to determine whether an RNAi antiviral response has occurred is to detect the production of vsiRNA. Previous studies have detected vsiRNA in invertebrate cells or mammalian cells with IFN system defects [29–31]. It is gratifying that more and more research has found the detection of vsiRNA in mammalian cells [25, 32, 33]. Moreover, when we infected macrophages with AIV-H9N2 or IBV-QX, the small RNA sequencing and vsiRNA analysis data of the macrophages revealed an interesting phenomenon (Fig. 1E and Supplementary Fig. S1C and D). The statistical results regarding vsiRNA quantities indicated that both the AIV-H9N2 and IBV-QX groups exhibited a measurable amount of vsiRNA. In the AIV group, negative-strand vsiRNA was predominant, whereas in the IBV group, positive-strand vsiRNA was more prevalent. Meanwhile, the vsiRNA reads showed a peak in 21 nt size for both groups (Fig. 1F–I). The above results indicated that infection of macrophages with two respiratory RNA viruses (AIV and IBV) in birds can induce the production of vsiRNA and RNAi antiviral immunity.

VsiRNA silences cognate viral RNA and inhibits virus replication

The distribution of vsiRNA in the viral genome can truly reflect the host's antiviral ability and preference to cleave viral dsRNAs. The distribution of vsiRNA in the AIV-H9N2 group is mainly concentrated in the HA, NP, NA, M, and NS gene regions (Fig. 2A), while in the IBV-QX group, vsiRNAs are distributed primarily on the non-structural protein 8 (NSP8), NSP9, and N gene regions (Fig. 2B). Subsequently, we selected three abundant vsiRNAs from the AIV and IBV groups for antiviral experiments. The western blotting results showed a significant decrease in the content of AIV-NP protein and IBV-N protein, indicating that transfection of the AIV group doubles-stranded vsiRNA (1, 2, and 3) and IBV group double-stranded vsiRNA (1, 2, and 3) can exhibit excellent anti-AIV and anti-IBV ability (Fig. 2C and D and Supplementary Fig. S2A-S2B). In order to further investigate the antiviral ability of homologous siRNA (+), complementary siRNA (-), and double-stranded RNA (±), we selected the third vsiRNA from the AIV and IBV groups for another antiviral experiment. The western blotting results showed that transfection of vsiRNA (-) and vsiRNA (±) in HD11 cells had a good inhibitory effect on the virus, while the effect of vsiRNA (+) was not significant (Supplementary Fig. S2C and D). To better apply it in cells and animals in the future, vsiRNA fragment was inserted into the psilencer4.1 vector through enzyme digestion and homologous grouping methods and obtained the PS-vsiRNA plasmid, which can efficiently express double-stranded vsiRNA (Supplementary Fig. S2E). As we can see, western blotting results also showed that the PS-vsiRNA plasmid (1, 2, and 3) had strong antiviral activity in both the AIV-H9N2 and IBV QX groups (Fig. 2E and F and Supplementary Fig. S2F and G).

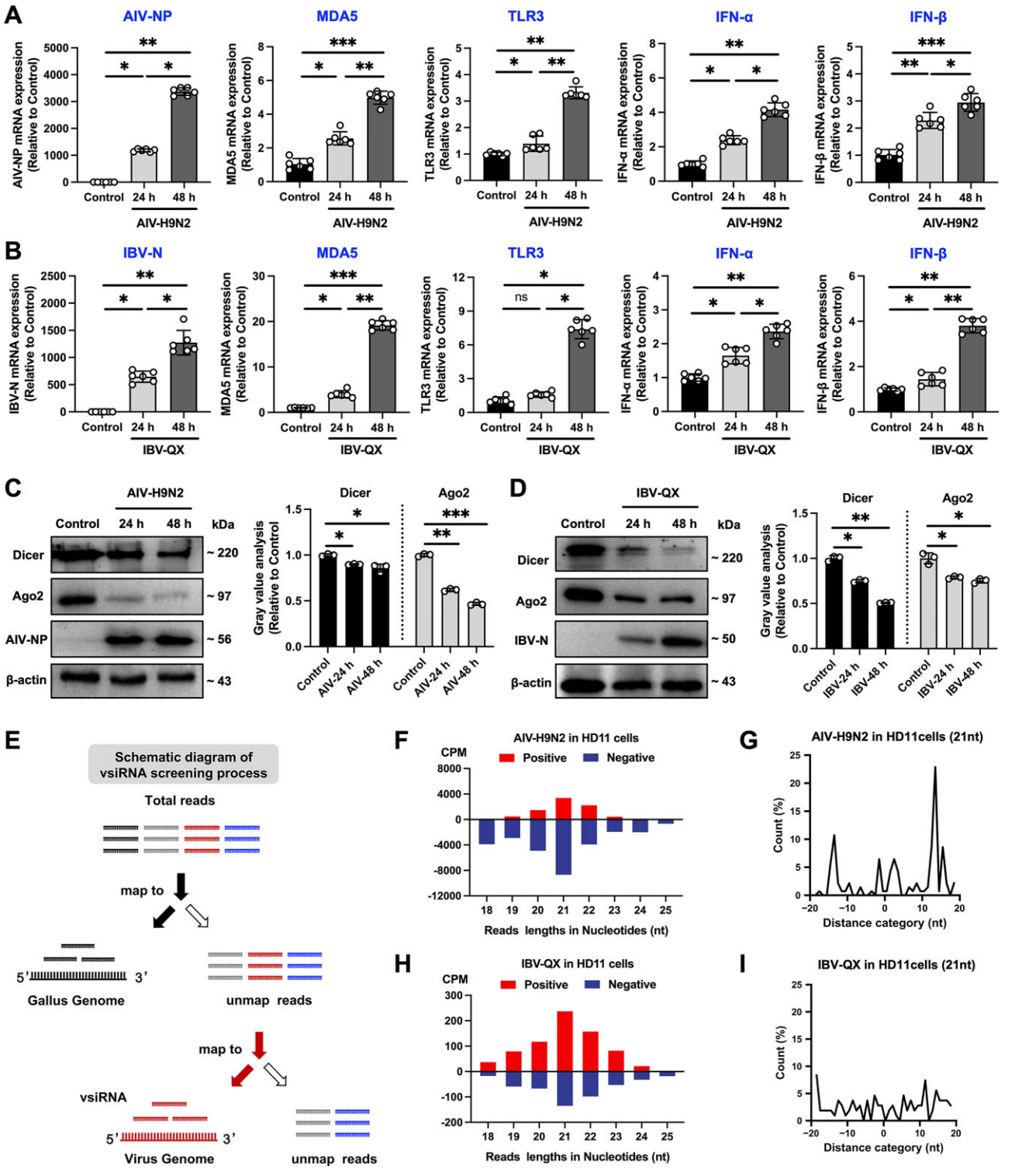

Figure 1. AIV and IBV infection triggers the production of vsiRNA in macrophages. (**A** and **B**) HD11 cells were infected with AIV-H9N2 (**A**) at MOI 1 and IBV-QX (**B**) at MOI 5, with the uninfected cells as the Control group. qRT-PCR was used at the indicated time point (24 h and 48 h) to assess the relative mRNA expression of AIV-NP, IBV-QX, MDA5, TLR3, IFN-α, and IFN-β. Data show expression calculated relative to β-actin and depicted as fold change relative to the Control group, normalized to 1. C and D: Western blotting was used for the AIV-NP (**C**), IBV-N (**D**), Dicer, and Ago2 detection. The loading control protein is β-actin, and the grey analysis is on the right. E: Flowchart of the vsiRNA analysis process for AIV and IBV groups. HD11 cells were infected with 1 MOI AIV-H9N2 and 5 MOI IBV-QX for 24 h. RNA extracts were prepared and subjected to RNA sequencing. Filter out the small RNAs matching the host genome, then compare the remaining small RNAs with the viral genome. F-I: Size distribution and abundance (counts per million of total reads, CPM) of 18–25 nt AIV-H9N2 (**F**) and IBV-QX (**H**) vsiRNA. Frequency of each distance category between 5′- and 3′-ends of a 21 nt complementary AIV-H9N2 (**G**) and IBV-QX (**I**) vsiRNA pair. Data are shown as the mean ± SD, $n = 3$. The differences were not significant at $P \geq 0.05$ (ns) or significant at $P < 0.05$ (*), $P < 0.01$ (**), $P < 0.001$ (***).

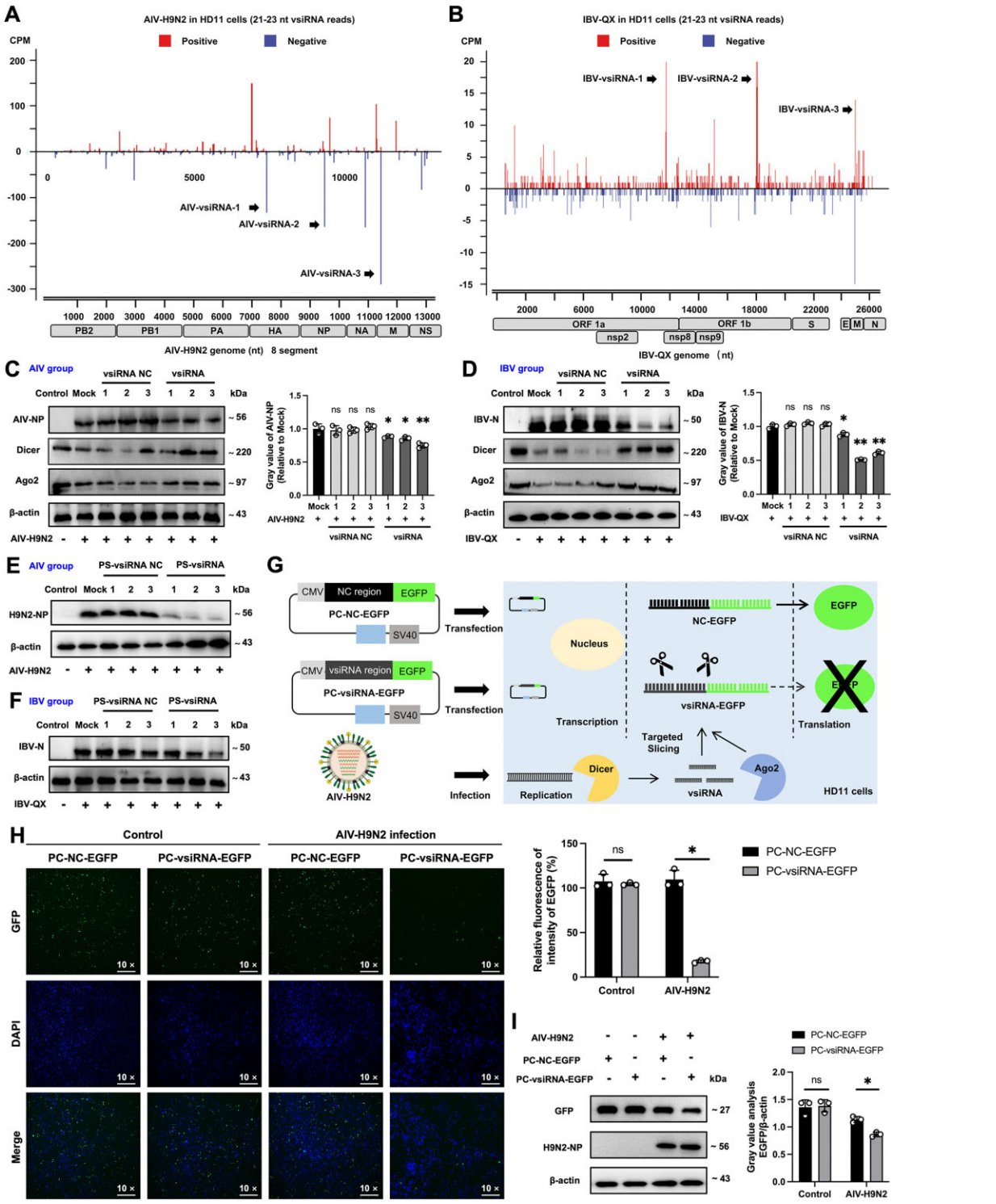

Figure 2. VsiRNA silences cognate viral RNA and inhibits virus replication. (**A**-**B**) The distribution and abundance map of 18–25 nt and 21–23 nt (+)- and (-)-stranded vsiRNA in the viral genome of AIV (**A**) and IBV (**B**) groups. (**C**-**D**) The western blotting results showed the antiviral effect of double-stranded vsiRNA in the AIV (**C**) and IBV (**D**) groups, as shown in the greyscale analysis on the right. The uninfected cells were marked as the Control group. β-actin was used as an internal reference protein, and the expression level of the Mock group (AIV-H9N2 positive control group) was set to "1," while the expression levels of other groups were multiples of the Mock group. It is worth noting that the vsiRNA and vsiRNA NC sequences of the AIV and IBV groups are different, as shown in Supplementary Table S3 for sequence information. (**E**-**F**) The western blotting results showed the antiviral effect of PS-vsiRNA in the AIV (**E**) and IBV (**F**) groups. (**G**-**I**) Fluorescence attenuation test mode diagram (**G**). HD11 cells were transfected with PC-vsiRNA-EGFP and PC-NC-EGFP for 12 h, then infected the 1 MOI AIV-H9N2 and subjected to fluorescence to detect the GFP expression for 24 h. The PC-NC-EGFP group was used as the negative control, and the right for the fluorescence intensity analysis. Besides, the fluorescence expression level of the PC-NC-EGFP Control group was set to "1," while the expression levels of other groups were multiples of the PC-NC-EGFP Control group (**H**). Western blotting result for the AIV group GFP expression in HD11 cells infected with AIV-H9N2 after transfected with PC-vsiRNA-EGFP, and PC-NC-EGFP as the control. The right figure shows the grey value analysis (I). Data are shown as the mean ± SD, $n = 3$. The differences were significant at $P < 0.05$ (*), $P < 0.01$ (**), or not significant at $P \geq 0.05$ (ns).

To further investigate whether gene silencing is caused by virus-induced vsiRNA targeting viral fragments, we designed a green fluorescence attenuation assay linked by vsiRNA targeting fragments and EGFP. The 90 bp AIV-H9N2 virus sequence, which contains the vsiRNA-targeted sequence, was inserted into the pcDNA3.1-EGFP-C (PC) plasmid that could express the EGFP protein (Supplementary Fig. S3A). HD11 cells were transfected with PC-vsiRNA-EGFP and PC-NC-EGFP for 12 h, and then infected the 1 MOI AIV-H9N2 and subjected to fluorescence to detect the GFP expresson for 24 h (Fig. 2G). The fluorescence microscopy results demonstrated that the expression level of GFP protein in the PC-vsiRNA-EGFP group decreased following AIV-H9N2 infection (Fig. 2H and Supplementary Fig. S3B), and the western blotting result also corroborated this finding (Fig. 2I). In addition, we also designed a double-stranded vsiRNA-targeted silencing PC-vsiRNA-EGFP assay to further validate the results of the virus group (Supplementary Fig. S4A). Both western blotting and fluorescence assay results showed that vsiRNA can target viral homologous fragments and lead to a decrease in EGFP expression (Supplementary Fig. S4B–D). Overall, these results indicate that vsiRNA can effectively target and silence homologous RNA (Fig. 2C–I).

The production and function of vsiRNA depend on the dicer-Ago2-vsiRNA axis

Dicer and Ago2 proteins are primarily responsible for the silencing effect of RNAi. We conducted HD11 cell knockout studies and subsequent complementation experiments to verify whether the vsiRNA synthesis and function are Dicer- and Ago2-dependent. Firstly, the western blotting results showed the successful construction of Dicer knockout cells (Dicer $^{-/-}$ HD11 cells) and Ago2 knockout cells (Ago2 $^{-/-}$ HD11 cells) (Fig. 3A and Supplementary Fig. S5A and B). Secondly, we found that the expression level of GFP protein and the intensity of green fluorescence did not decrease in Dicer $^{-/-}$ HD11 cells and Ago2 $^{-/-}$ HD11 cells (Fig. 3B-C and Supplementary Fig. S5C–E). Following this, we constructed overexpression plasmids of Dicer and Ago2, and western blotting results confirmed the successful construction of these plasmids (Fig. 3D and Supplementary Fig. S6A and B). Thirdly, we transfected PC-Dicer and PC-Ago2 into the respective knockout cells for complementation. Fluorescence analysis indicated a moderate decrease in fluorescence quantity and intensity following complementation with Dicer and Ago2 (Fig. 3E and Supplementary Fig. S6C and D). Fourthly, we also observed significantly elevated mRNA levels of AIV and IBV following Dicer and Ago2 knockout (Fig. 3F). Upon overexpression of Dicer and Ago2, the NP protein levels of AIV-H9N2 were significantly reduced (Fig. 3G). Meanwhile, we also have supplemented the proposed RNA sequencing, as shown in Supplementary Fig. S6E and F. Indeed, the number of vsiRNA increased after transfection of PC-Dicer and PC-Ago2 in knockout cells. In conclusion, vsiRNA production and silencing are mediated by the Dicer-Ago2-vsiRNA axis, which plays a crucial role in combating RNA viruses.

A conserved RWM motif for the vsiRNA production

The large-scale analysis of vsiRNA based on their antiviral efficacy is of great significance for broad-spectrum antiviral therapy. Firstly, we used the National Center for Biotechnology Information (NCBI) GEO database to download small RNAs sequencing data produced by bird RNA virus infected cells or animal tissues, and performed vsiRNA statistical analysis on this portion of small RNAs. As we can see, vsiRNA can also be detected in the group of AIV-H9N2 infected dendritic cells, and the generated vsiRNA is mostly negative chain (Fig. 4A–C). Interestingly, vsiRNA also can be found in the NDV group, with the high-virulence strain F48E9 having more vsiRNA than the low-virulence strain LaSota (Fig. 4D–F and Supplementary Fig. S7A-S7B). Besides, the number of vsiRNA in the chicken infectious bursal disease (IBDV) group is also significant, and the abundance of vsiRNA is higher at the 5′ and 3′ terminus (Fig. 4G–I). The information above demonstrated that RNA virus-infected avian cells and tissues can detect vsiRNA production. Strangely, vsiRNA was also not detected in the bovine viral diarrhea mucosal disease virus (BVDV) and bovine respiratory syncytial virus (BRSV) groups of ruminant-related viruses. However, a large number of vsiRNAs can be detected in the Bluetongue Virus (BTV) group and are concentrated in the 804 bp gene region at the 3′ terminus (Supplementary Fig. S7C–E). Besides, we also analyzed the SARS-CoV-2 related vsiRNA, which were mainly divided into the Caco-2 cell group, A549-ACE2 cell group, and human small airway epithelial cells (SAECs) group. A large number of vsiRNA can be observed in the Caco-2 cell group and A549-ACE2 cell group, and this part of vsiRNA is mainly concentrated in the ORF1 and structural protein gene regions, such as the N gene (Supplementary Fig. S8A–F). It is worth pondering that there is only a small amount of vsiRNA in the SAECs cell group, and they are scattered in various regions (Supplementary Fig. S8G–H). However, the antiviral testing of this part of vsiRNA for SARS-CoV-2 needs to be validated. As for whether other animal viruses will produce vsiRNA after infecting cells or animal tissues, it is still a mystery that needs further research to explore.

A conserved GYM motif involved in miRNA detection and cleavage was discovered in a recent study [34, 35]. Therefore, we nested Homo sapiens, Sus scrofa, Bos taurus, Ovis aries, Gallus, Danio rerio, and Drosophila miRNA into this motif for scoring. Dicer cleaved Pre-miRNA into the miRNA in most of these species, in accordance with this conserved "GYM" motif (Fig. 5A). We then wondered whether there is a specific sequence recognition motif in vsiRNA. We created an vsiRNA database and examined the vsiRNA sequence bases after 21–23 nt vsiRNA were screened (Fig. 5B). The findings show that bases A and U are preferred at the 5′ and 3′ terminus of vsiRNA (Fig. 5C). Screening the coordinates with significantly more initial reads, we took the bases within 6 bp upstream and downstream of these sites to form a new fasta file, which was then imported into logo to generate the corresponding motif. We found a position-dependent 3 bp motif that strongly promotes processing: a paired purine A or G (R), a mismatched A or less favorably U (W), and a paired A or U (M) at positions -1, 0, and 1 on the 3p side, respectively. We named this element the RWM motif and it had a clear consensus sequence. The RWM motif promotes processing at a specific position to produce vsiRNA (Fig. 5D). To evaluate the effectiveness of generating vsiRNA based on RWM motif cutting, we conducted anti-AIV-H9N2 experiments on vsiRNA that conform to different RWM motifs. The results of the plaque test showed that vsiRNA that maximally conforms to the RWM motif has better antiviral effects, indirectly indicating that Dicer has a preference for cutting vsiRNA that conforms to the RWM motif (Fig. 5F and G).

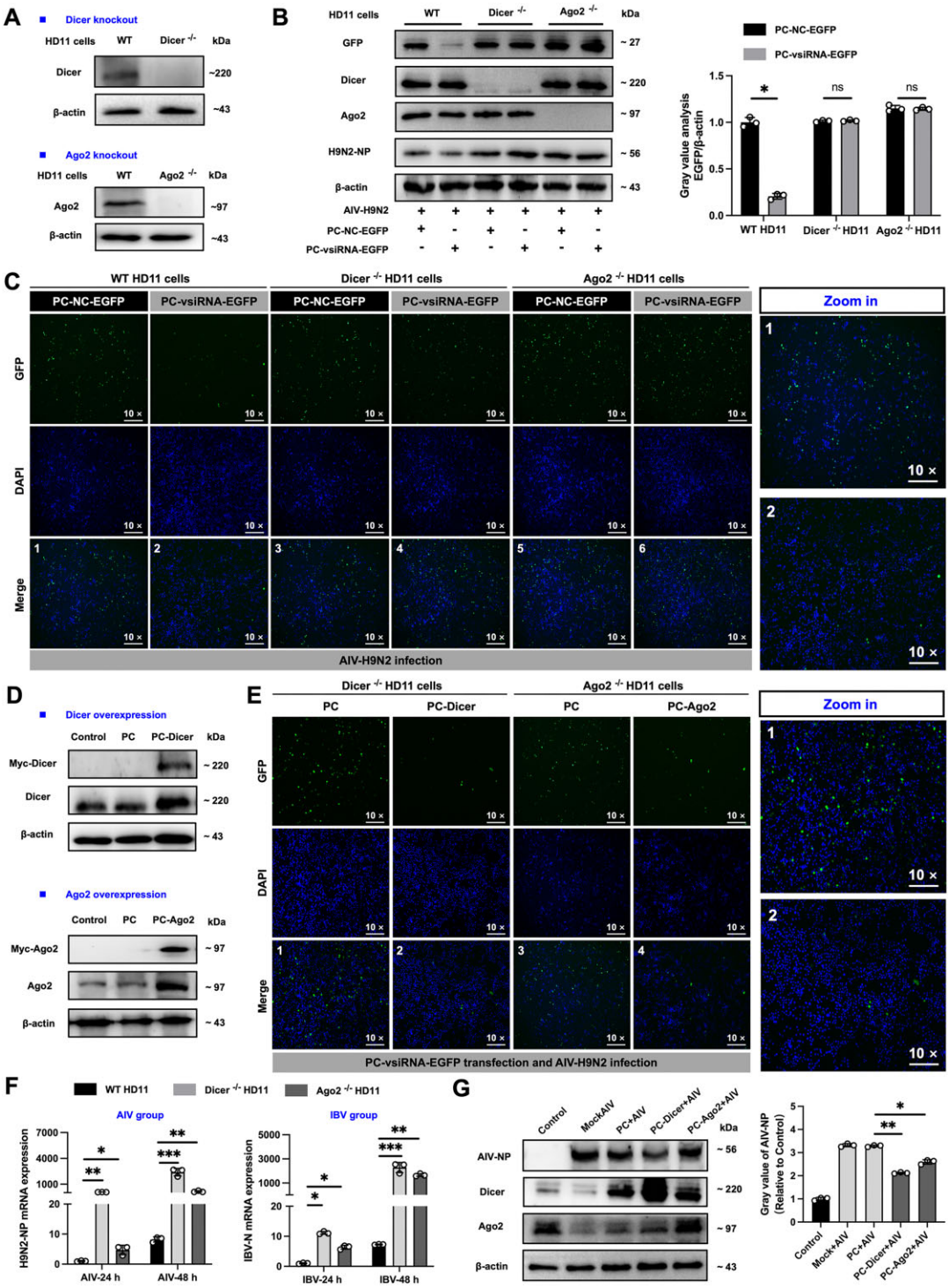

Figure 3. The production and function of vsiRNA depend on the Dicer-Ago2-vsiRNA axis. (**A**) Western blotting detection of the knockout effect of Dicer and Ago2 proteins in Dicer knockout (Dicer $^{-/-}$) HD11 cells and Ago2 knockout (Ago2 $^{-/-}$) HD11 cells. (B-C) WT HD11 cells, Dicer $^{-/-}$ HD11 cells, and Ago2 $^{-/-}$ HD11 cells were transfected with PC-vsiRNA-EGFP and PC-NC-EGFP for 12 h, then infected the 1 MOI AIV-H9N2 and subjected to western blotting (**B**) and fluorescence (**C**) to detect the GFP expression for 24 h. The "WT HD11 cells transfected PC-NC-EGFP group" was used as the control and the right for the grey value analysis. Besides, the grey value expression of EGFP for the "WT HD11 cells transfected PC-NC-EGFP group" was set to "1," while the expression levels of other groups were multiples of this group. Fluorescent protein represents the the GFP, while DAPI stained represents the nucleus, 10×. (**D**) Western blotting detection of the overexpression effect of Dicer and Ago2 proteins in the HD11 cells after transfected the PC-Dicer and PC-Ago2 plasmid for 48 h. (**E**) Fluorescent result of the Dicer $^{-/-}$ HD11 cells and Ago2 $^{-/-}$ HD11 cells were transfected with the PC-Dicer, PC-Ago2, and pcDNA3.1(+)/myc-His B (PC) plasmid for 12 h. The PC group is the negative control for the overexpression. Subsequently, after transfecting the PC-vsiRNA-EGFP plasmid for 12 h and then infecting the 1 MOI AIV-H9N2, we subjected to fluorescence to detect the GFP expression for 24 h. (**F**) WT HD11 cells, Dicer $^{-/-}$ HD11 cells and Ago2 $^{-/-}$ HD11 cells were infected with AIV-H9N2 (1 MOI) and IBV-QX (5 MOI). qRT-PCR was used at the 24 h and 48 h time point to assess the relative mRNA expression of AIV-NP and IBV-QX. (**G**) The efficacy of PC-Dicer and PC-Ago2 against AIV-H9N2 was detected by western blotting, the right for the grey value analysis. Data are shown as the mean ± SD, n = 3. The differences were not significant at $P \geq 0.05$ (ns) or significant at $P < 0.05$ (*), $P < 0.01$ (**), $P < 0.001$ (***).

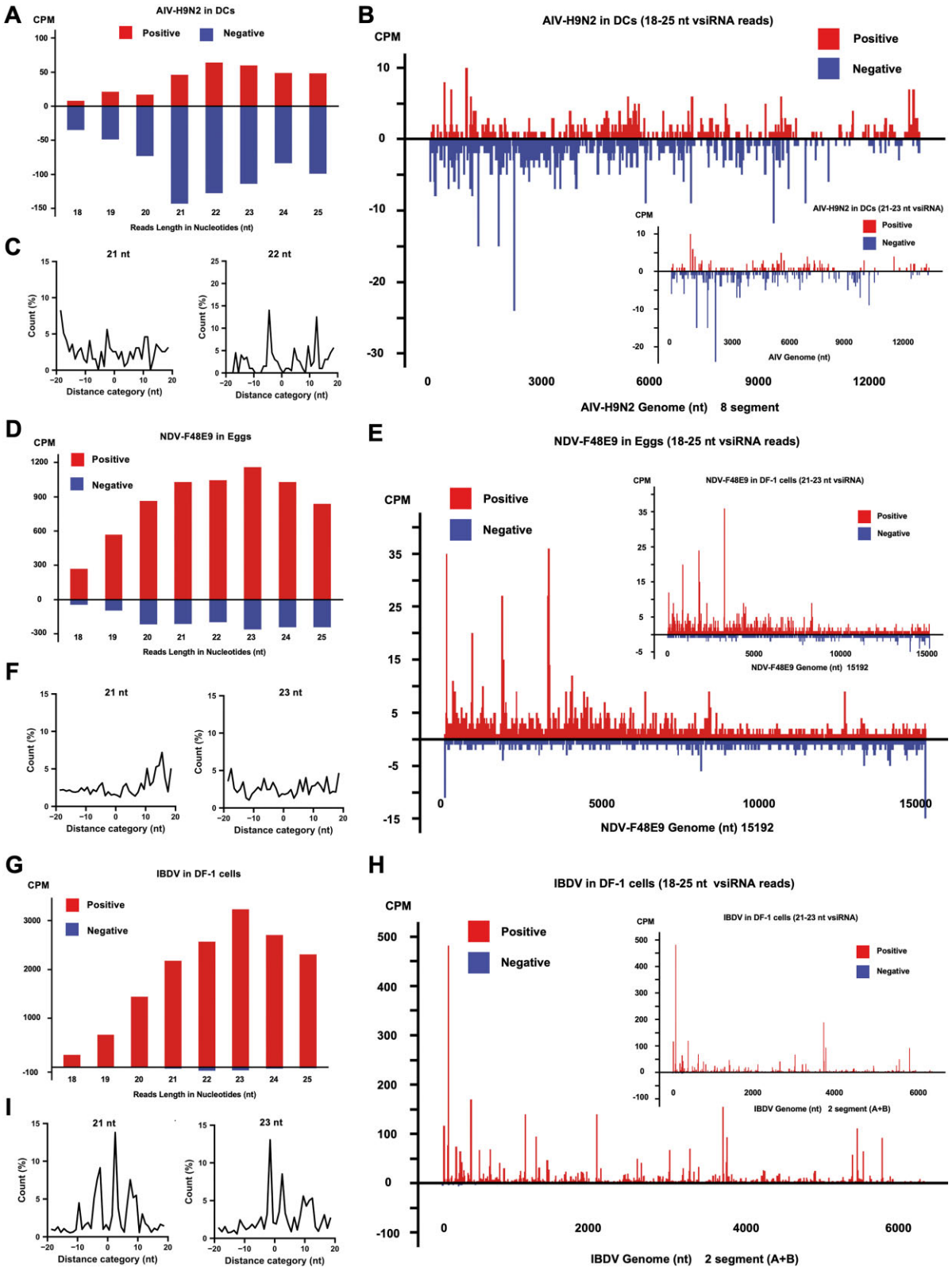

Figure 4. VsiRNA can be detected in cells and tissues infected with other avian RNA viruses. (**A**-**C**) Chicken dendritic cells (DCs) were infected with the AIV-H9N2 (10^6 $TCID_{50}$/0.1 mL) for 6 h. (**A**) Size distribution and abundance (CPM) of total AIV-H9N2 vsiRNA. The Upper represents the (+)-stranded vsiRNA and lower represents (-)-stranded vsiRNA. (**B**) The distribution and abundance of 18–25 nt and 21–23 nt reads included (+)- and (-)-stranded in the AIV-H9N2 genome are indicated. (**C**) Frequency of each distance category between 5′- and 3′-ends of a 21 nt and 22 nt complementary AIV vsiRNA pair. (**D**-**F**) Eggs were infected with NDV-F48E9 (10^4 PFU) for 36 h. (**D**) Size distribution and abundance (CPM) of total NDV-F48E9 vsiRNA. (**E**) The distribution and abundance of 18–25 nt and 21–23 nt reads included (+)- and (-)-stranded in the NDV-F48E9 genome are indicated. (**F**) Frequency of each distance category between 5′- and 3′-ends of a 21 nt and 23 nt complementary NDV-F48E9 vsiRNA pair. (**G**-**I**) DF-1 cells were infected with IBDV (1 MOI) for 24 h. (**G**) Size distribution and abundance (CPM) of total IBDV vsiRNA. (**H**) The distribution and abundance of 18–25 and 21–23 nt reads in (+)- and (-)-stranded IBDV genomes are indicated. (**I**) Frequency of each distance category between 5′- and 3′-ends of a 21 and 23 nt complementary IBDV vsiRNA pair.

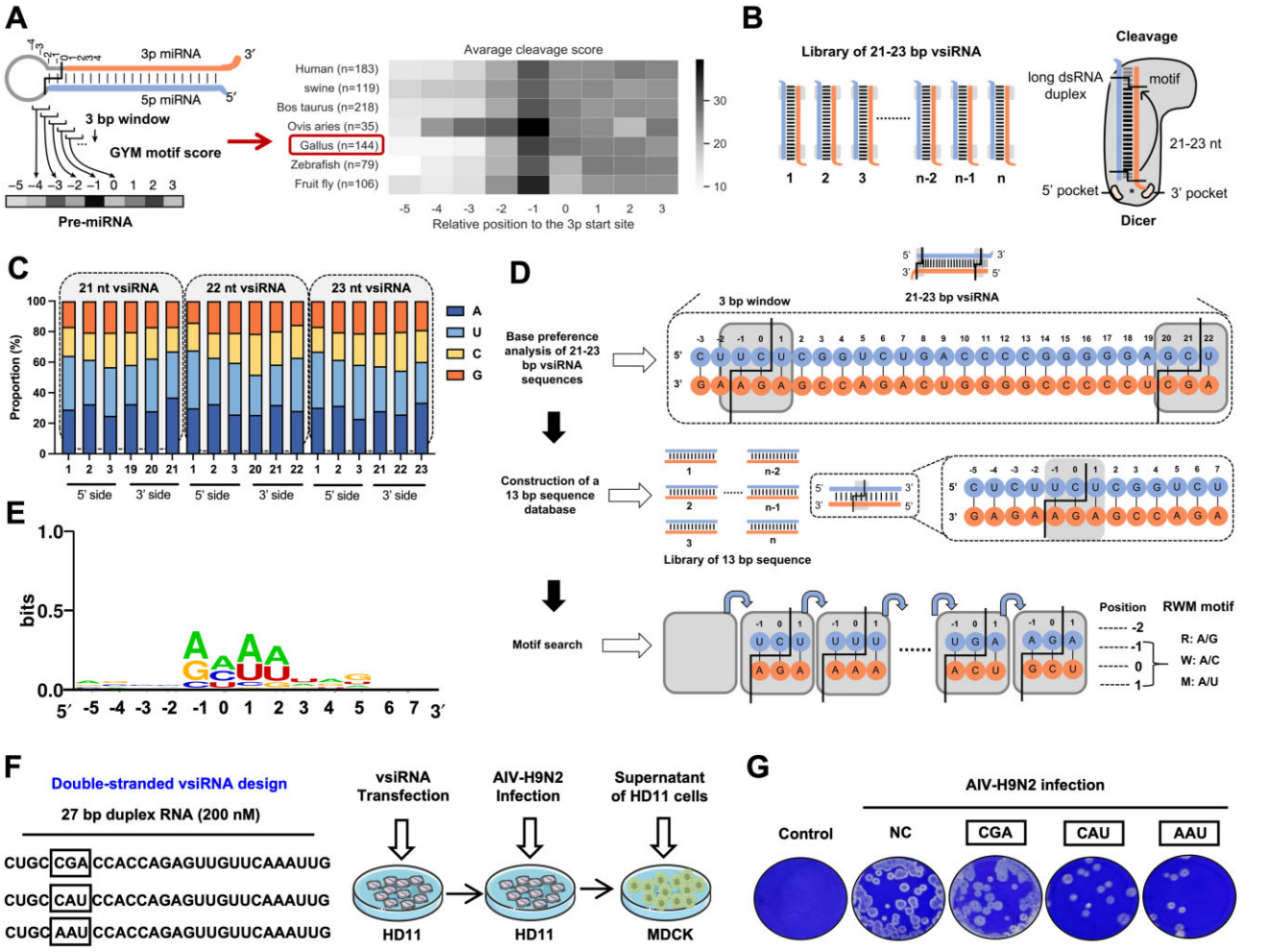

Figure 5. A conserved RWM motif for the vsiRNA production. (**A**) The scoring of the "GYM" motif following the *Young-Yoon Lee* paper [34, 35]. Additional part: Download pre-miRNA data from databases such as miRBase and miRgeneDB for Sus scrofa (Swine), Bos taurus, Ovis aries, and Gallus for the "GYM" motif score analysis. (**B**) Construct a total vsiRNA database from all vsiRNA detected in this manuscript. (**C**) Perform base bias analysis on 21–23 nt vsiRNA in the vsiRNA database. (**D**-**E**) The vsiRNA motif screening process diagram (**D**). The "RWM" motif recognizes the cleavage mode, where R represents the approximate rate of A/G, W represents A/C, and M represents A/U (**E**). (**F** and **G**) Choose CGA, CAU, and AAU motifs in combination with AIV-H9N2 vsiRNA3 for RWM motif cutting validation (**F**). After transfecting RWM motif double-stranded vsiRNA (200 nM) into HD11 cells, infection was carried out using 1 MOI AIV-H9N2, and the cell supernatant was collected and incubated with the MDCKs for plaque detection assay (**G**). Data are shown as the mean ± SD, $n = 3$.

DicerM is a novel antiviral Dicer isoform in bird

It is well known that one or more Dicer proteins are responsible for the production of small RNA in eukaryotes and indicated that a novel Dicer isoform in mammalian stem cells (AviD) and oocytes (DicerO) functions in viral defense [36, 37]. The gallus-Dicer protein was discovered to be very similar to that of mammals when we compared it with the Dicer of several other species and examined the genetic evolution tree (Fig. 6A). By analogy, we found that birds might also possess a Dicer isoform "DicerM," which lacks exon 9 and exon 10, compared to Dicer (Fig. 6B). Subsequently, we designed specific primers to clone distinct target bands for Dicer and DicerM in both SPF chickens and their related cells (Fig. 6C and D). Continued protein detection verified the Dicer and DicerM protein expression in HD11, DF-1, Chicken liver cancer cells (LMH), and PBMCs-Mφ (Supplementary Fig. S9A). To investigate the antiviral effects of Dicer and DicerM, we set up three siRNA targeting Dicer and DicerM (Fig. 6E and Supplementary Fig. S9B and C). qRT-PCR and western blotting results showed that the viral load of IBV was higher in the Dicer and DicerM silencing group than in the siNC group (Fig. 6F and Supplementary Fig. S9D–J). In addition, we also obtained similar results using the psilencer4.1 (PS) recombinant plasmid that can stably express siRNA (Supplementary Fig. S9E–I). According to the vsiRNA analysis results in Supplementary Fig. S6E and Fig. 2A, it can be seen that after Dicer/DicerM knockout, the number of vsiRNA significantly decreased, indicating that the production of vsiRNA is related to Dicer/DicerM. As for why there is still a small amount of vsiRNA produced in knock-out cells, the reason is that there are other nucleases such as RNaseL inside the cells that can cleave nucleic acids, but they also play a very minor role.

For the overexpression experiment, we constructed the DicerM overexpression plasmid pcDNA3.1-DicerM-his (PC-DicerM) and validated its expression through double enzyme digestion and fluorescence assays (Supplementary Fig. S10A–C). Following this, we found the overexpression of Dicer and

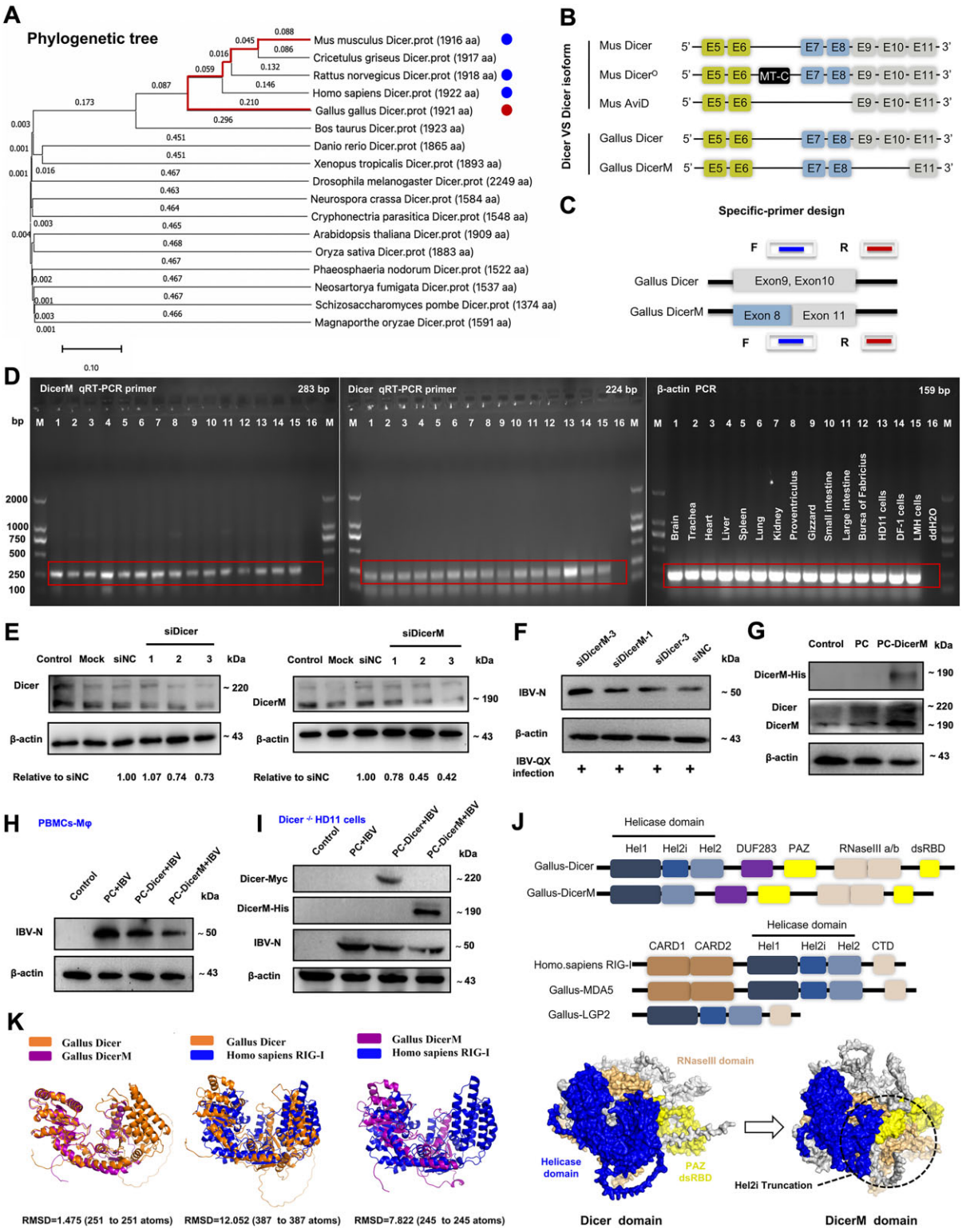

Figure 6. DicerM is a novel antiviral Dicer isoform in bird. (**A**) Genetic evolutionary tree of different species Dicer. (**B**) Comparison of the helicase domain of Dicer and Dicer-isoform. (**C-D**) Dicer and Dicer qRT-PCR primer design flowchart (**C**) and PCR detection result of SPF chicken tissues and chicken passable cells in our lab (**D**). β-actin was amplified as an internal reference gene. (**E**) Screening siRNA with better silencing effect on Dicer and DicerM through western blotting. (**F**) Transfected siNC, siDicer-3, siDicerM-1, and siDicerM-3 into HD11 cells for 12 h before conducting infection experiments using IBV-QX. After 24 h, detect the protein content of IBV-N by western blotting. β-actin was used as an internal reference protein, and the expression level of the siNC group was set to "1," while the expression levels of other groups were multiples of the siNC group. (**G**) The expression was verified by western blotting after transfection with PC-DicerM for 48 h. H and I: The anti-IBV efficacy was verified by western blotting after transfection with PC-Dicer and PC-DicerM in PBMCs-Mφ (**H**) and Dicer $^{-/-}$ HD11 cells (**I**). (**J-K**) Protein structure analysis Gallus-Dicer, Gallus-DicerM, Homo sapiens RIG-I, Gallus-MDA5, and Gallus-LGP2 helicase domain (**J**). Analysis of the similarity of Gallus-Dicer, Gallus-DicerM, and Homo sapiens RIG-I helicase using PyMOL software, and the results shown with the RMSD. The lower the RMSD is the greater the similarity (**K**). Data are shown as the mean ± SD, $n = 3$.

DicerM could effectively reduce IBV viral load on PBMCs-Mφ, even in the Dicer $^{-/-}$ HD11 cells (Fig. 6H and I and Supplementary Fig. S10D and E). In addition, the Dicer isoform "DicerM" also has good anti-AIV-H9N2 and anti-IBDV effects on DF-1 cells (Supplementary Fig. S10F-S10G). Collectively, these findings suggest that DicerM also plays a critical role in inhibiting RNA virus replication, like the Dicer protein.

Alignment analysis of the helicase domains in RNA recognition receptor proteins

Previous studies in mammals have revealed that the Helicase (Hel) domain of AviD is closer to the dsRNA recognition receptors Retinoic acid-inducible gene-I (RIG-I), Melanoma differentiation-associated gene 5 (MDA5), and Laboratory of genetics and physiology 2 (LGP2) than Dicer, indicating the stronger antiviral ability of AviD in mammals compared to Dicer [36, 38]. DicerM executed its antiviral function mainly by recognizing and cleavaging dsRNA of RNA viruses. In birds, due to the lack of Gallus-RIG-I receptors, we compared Gallus-DicerM and Gallus-Dicer Hel domains with Homo sapiens RIG-I, Gallus-MDA5, and Gallus-LGP2. Results showed that the Hel domain was highly similar among the above-reported genes. Protein structure analysis found that Gallus-DicerM lacked the Hel2i and a portion of the Hel2 domain of the N-terminal segment than Gallus-Dicer (Fig. 6J). Further structure analysis of the helicase domain revealed that Gallus-DicerM was more similar to Homo sapiens RIG-1 (RMSD: 7.822) than Gallus-Dicer (RMSD: 12.052), indicating that Gallus-DicerM might be more efficient than Dicer in identifying virus dsRNA (Fig. 6K and Supplementary Tables S5 and S6).

Interactions between various dsRNA receptors

As we all know, the IFN system in higher organisms can generally inhibit Dicer recognition of dsRNA in RNAi via LGP2, such as in mammals [9, 39]. We wondered why RNAi performs better in birds. Therefore, we further investigate how the RNAi system (DicerM and Dicer) and IFN system (LGP2 and MDA5) interact with each other. The results showed that overexpression of DicerM induced a slight increase in mRNA and protein levels of LGP2 and MDA5 (Supplementary Fig. S10H and I). On the one hand, the above expression indicates that the expression of DicerM in the RNAi pathway does promote the expression of key RNA recognition receptor proteins in the IFN pathway. On the other hand, we further observe whether the IFN system has a certain impact on the RNAi system (Supplementary Fig. S11A and B). HD11 cells were transfected with the PC-LGP2 and PS-LGP2 for 48 h, and subjected to qRT-PCR and western blotting to detect the Dicer and DicerM expression. Results showed that the overexpression of the Gallus-LGP2 is beneficial for the expression of Dicer and DicerM, which is opposite to the results for mammals (Fig. 7A and Supplementary Fig. S11C–F). In contrast, after transfection with PS-LGP2, results showed that the silencing of LGP2 reduced the expression of Dicer and DicerM in HD11 cells. Interestingly, MDA5 also showed similar conclusions (Fig. 7B and Supplementary Fig. S11C–F). Meanwhile, the qRT-PCR and western blotting results show that the LGP2 and MDA5 overexpression can decrease the AIV-NP mRNA and protein expression (Fig. 7C and D and Supplementary Fig. S12A–D). These data hint that the expression of LGP2 and MDA5 plays an important role in reducing the load of AIV-H9N2 in macrophages.

Further, we conduct molecular docking experiments on DicerM/Dicer and LGP2/MDA5 (Fig. 7E and F and Supplementary Fig. S13A-D). The dock results show that HIS395 and HIS69, positive-strand with LGP2 protein (L), form salt bridge interactions with GLU582 and GLU1507, negative-strand with DicerM protein (A). LY2577, ASP583, GLU582, LYS618, ASN879, GLN1511, GLU1507, and ARG1624 of DicerM protein form hydrogen bonds with ARG72, HIS69, GLU2, ASP387, GLY393, HIS395, GLU429, GLU447, and CYS1640 of LGP2 protein (Fig. 7E and F). In addition, the positive-strand ARG1362 of DicerM (A) interacts with the negative-strand 841 of MDA5 protein (M) to form a salt bridge, while the negatively charged ASP1124 and ASP395 of DicerM protein interact with the positively charged ARG834 and LYS537 of MDA5 protein to form a salt bridge. ASP395, GLU443, and ASP237 of DicerM protein form hydrogen bonds with LYS537, VAL226, and ARG422 of MDA5 protein (Supplementary Fig. S13C and D). More importantly, we also conducted IP experiments, and the results showed that Dicer and DicerM both interacted with LGP2, but not with MDA5 (Fig. 7G and H). As for which joint domain of Dicer and DicerM interacts with LGP2, it is worth further exploring in the future. Together, the bird RNAi system is closely connected to the IFN system, playing a synergistic role *in vivo*.

Antiviral application of PS-vsiRNA plasmid

Previous studies have shown the importance of RNAi in the antiviral process of bird [35, 36]. Therefore, based on GWM motif screening, we conducted antiviral validation using AIV group vsiRNA target region (M and NS1) and IBDV group vsiRNA target region (VP5 an VP3). The data shows specific screening and regions used for plasmid construction (PS-VP3 and PS-NS1) through pattern diagrams (Fig. 8A). Transfection of PS-M-NS1 plasmid in DF-1 cells can reduce the viral load of AIV-H9N2 (Fig. 8B-C and Supplementary Fig. S14A and B). Besides, the results of the western blotting, plaque test, and qRT-PCR also demonstrated that PS-VP5-VP3 can lower IBDV load level, hence preventing IBDV from proliferating and replicating (Fig. 8D and E and Supplementary Fig. S14C and D). In a clinical setting, we combined the PS-M-NS1 plasmid or the PS-VP5-VP3 plasmid with nanomaterial polyetherimide (PEI) and made it to the PEI/PS-viRNA polyplex nanoparticles (PPvPNs). The nanoparticle size analysis showed that the size of PPvPNs was 116.1 nm, and the Zeta potential result showed that it was 18.3 mV, indicating good positive charge characteristics for better adhesion to mucous membranes (Supplementary Fig. S14E and F). Finally, we also administered the PPvPNs to SPF chickens by nasal drip twice and the infection test after the second immunization (Fig. 8F). PS-M-NS1 plasmid group can alleviate AIV-H9N2-related lung inflammation, hemorrhage, and other ailments (Fig. 8G). Results from the bursa of Fabricius morphology and HE staining revealed that the PS-VP5-VP3 immune group can lower the IBDV viral load and shield immunized hens after employing IBDV to battle the virus (Fig. 8H and Supplementary Fig. S14G). In conclusion, the vsiRNA-based prevention and control strategy using PS-vsiRNA plasmid in conjunction with PEI worked well.

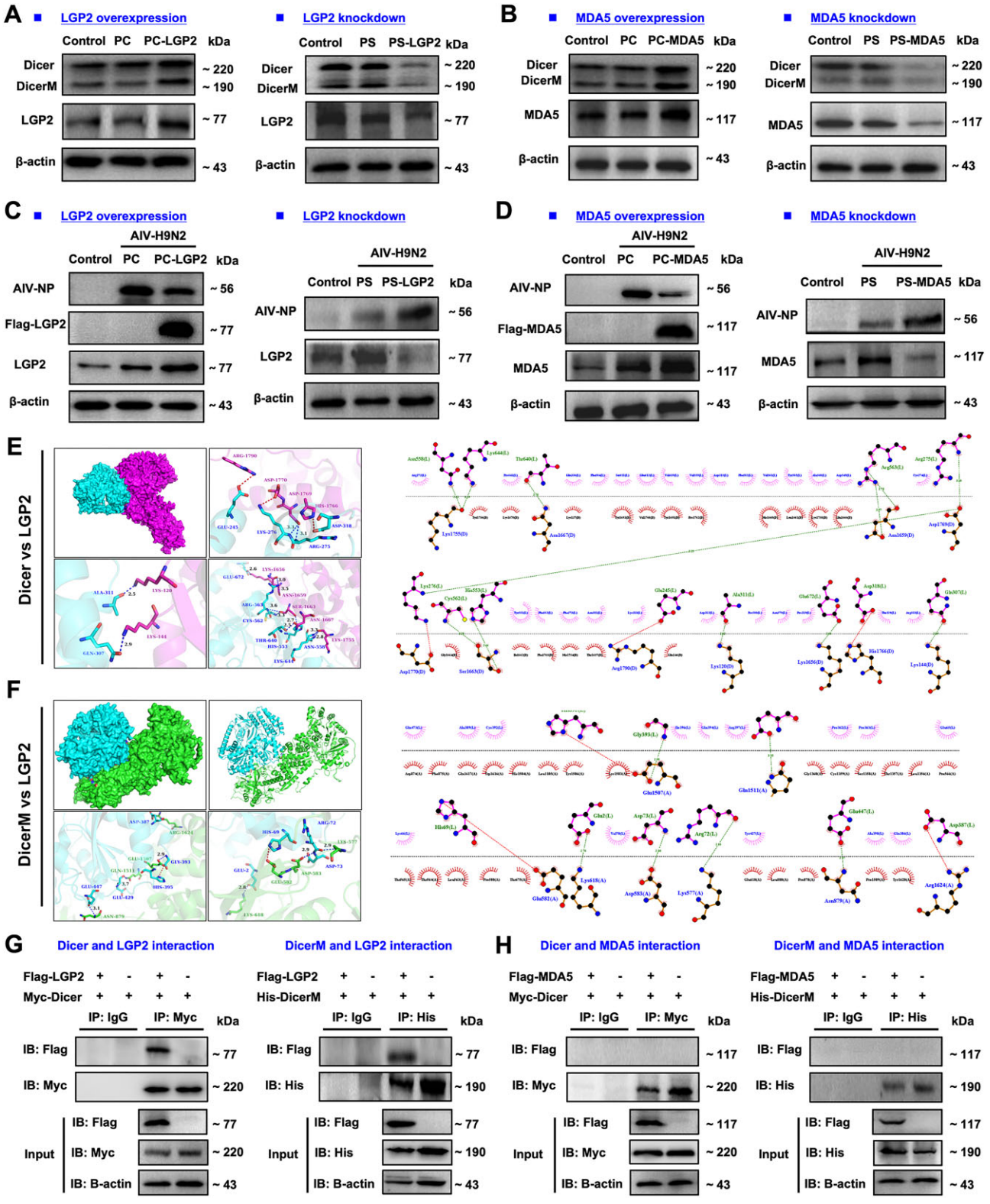

Figure 7. Interactions between various dsRNA receptors. (**A**-**B**) The effect of LGP2 (**A**) and MDA5 (**B**) overexpression and silencing on the expression levels of Dicer and DicerM was detected by western blotting assay. C-D: HD11 cells were transfected with the PC-LGP2, PS-LGP2 (**C**), PC-MDA5, and PS-MDA5 (**D**) for 24 h, and then infected with 1 MOI AIV-H9N2 and subjected to western blotting to detect the AIV-NP expression for 24 h. The uninfected cells as the Control group. β-actin was used as an internal reference protein, and the expression level of the Control group was set to "1," while the expression levels of other groups were multiples of the Control group. Notably, the pcDNA3.1 (PC) group and the psilencer4.1 (PS) group were used as the transfection control (negative). E-F: The three-dimensional and two-dimensional molecular docking results of LGP2&Dicer (**E**) and LGP2&DicerM (**F**), where L represents LGP2, D represents Dicer and A represents DicerM. G-H: The PC-Dicer, PC-DicerM, PC-LGP2, and PC-MDA5 were co-transfected into 293T cells in a 1:1 ratio. After 24 h, collect cell samples according to the Co-IP Kit. Myc, His, IgG for IP, and the input for the Flag and His antibodies, β-actin for the reference control. Data are shown as the mean ± SD, $n = 3$.

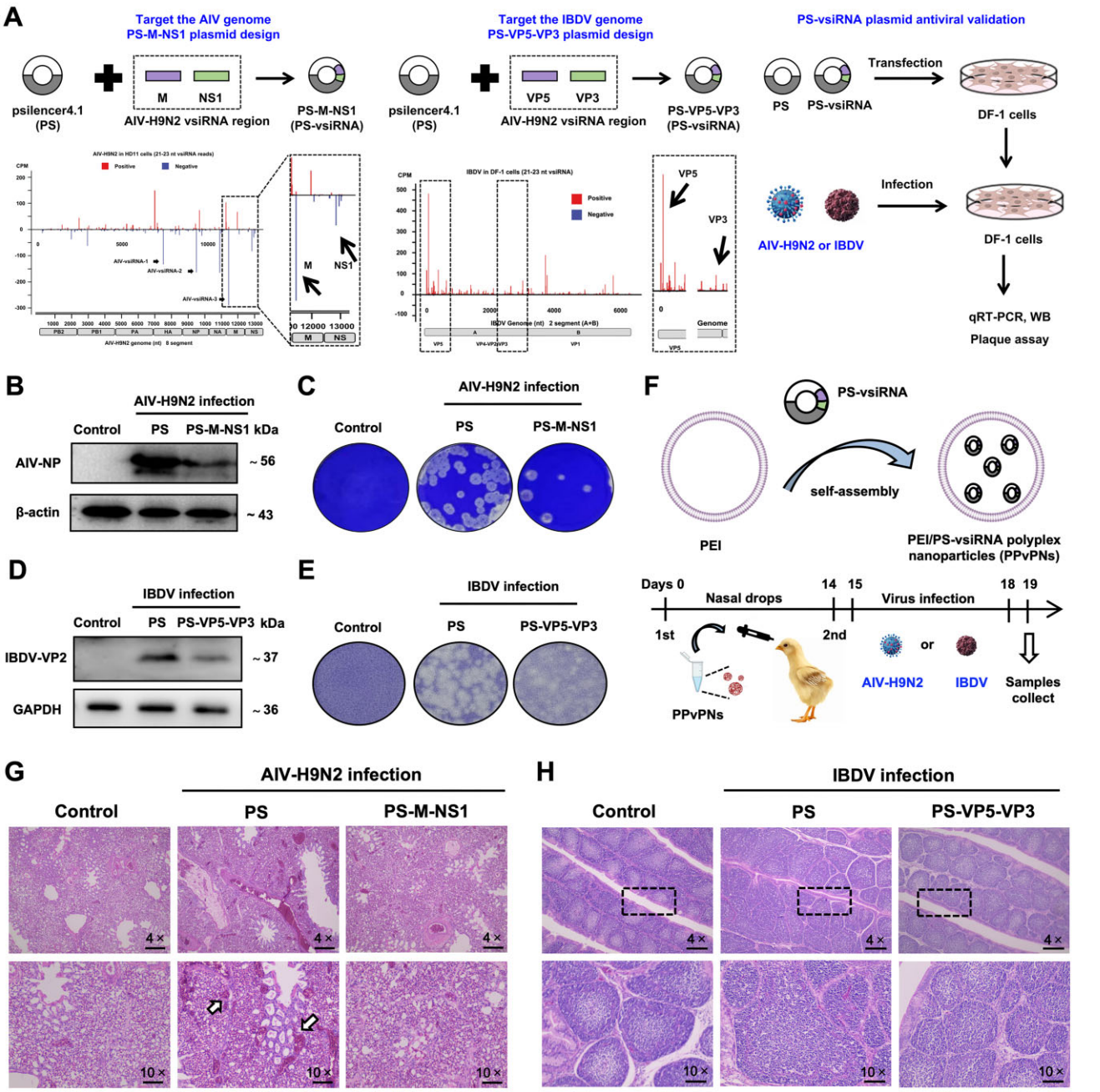

Figure 8. Antiviral validation of vsiRNA using motif screening. (**A**) The flowchart of the PS-M-NS1 and PS-VP5-VP3 plasmid screening and antiviral test. DF-1 cells were transfected with the PS, PS-M-NS1, and PS-VP5-VP3 for 12 h, and then infected with the 1 MOI AIV-H9N2 and 0.1 MOI IBDV. qRT-PCR, western blotting, and plaque assay were used to detect the AIV load for 24 and 48 h. (**B** and **C**) Verify the protective effect of PS-M-NS1 on DF-1 cells through western blotting (**B**) and plaque assay (**C**). The uninfected cells are the Control group. β-actin was used as an internal reference protein, and the expression level of the Control group was set to "1," while the expression levels of other groups were multiples of the Control group. Notably, the psilencer4.1 (PS) group was used as the transfection control. (**D** and **E**) Verify the protective effect of PS-VP5-VP3 on DF-1 cells through western blotting (**D**) and plaque assay (**E**). PS group was used as the transfection control. (**F**) The mixture of PS-M-NS1 & PEI and PS-VP5-VP3 PEI were delivered to the chicken via nasal drip. Two weeks later, deliver the mixture of PPvPNs through nasal drip again. Conduct virus attack protection test on the 15th day of infusion and collect samples (lungs, bursa of Fabricius) for subsequent analysis on the 18th and 19th days. (**G** and **H**) Three days after the AIV and IBDV challenge, showing the HE staining of the lung (**H**) and bursa of Fabricius (**G**). The arrow indicates the bleeding area, and the box surrounds the space between the bursa of Fabricius. Data are shown as the mean ± SD, $n = 3$.

Discussion

A conserved gene-silencing mechanism called RNAi developed in various eukaryotes as a cell-intrinsic antiviral immune defense mechanism [40, 41]. Whether RNAi has an antiviral response function in vertebrates is still a research direction, and many studies have conducted various discussions on this, such as the existence of the IFN system and how much antiviral effect RNAi plays [42]. At the same time, a study has shown that although the IFN antiviral system exists, the RNAi antiviral defense system of the Ago protein is equally important, indicating the importance of exploring the RNAi antiviral system [43]. However, concerns regarding the role of RNAi antiviral immunity in mammals were raised by the absence of vsiRNA in virus-infected mammalian cells [31, 44, 45]. In mammals, only a tiny number of studies have detected vsiRNA in cells with relative deficiencies in the IFN system, such as stem cells and oocytes [46–48]. It is gratifying that based on the development of sequencing technology, many recent studies have shown that vsiRNA can be found in wild-type (WT) viruses-infected mammalian somatic cells, and this portion of vsiRNA has certain functions [26, 49, 50]. Retrospecting at bird, chickens lack important dsRNA recognition receptors RIG-I, resulting in relative deficiencies in the IFN system and susceptibility to RNA virus attacks [51, 52]. Therefore, an in-depth exploration of the relationship between RNAi antiviral immunity and RNA viruses in birds is of great significance for comprehensive prevention and control in the poultry industry.

IFN and RNAi are two crucial antiviral mechanisms, and their expression can illustrate the relationship between host antiviral resistance and viral immune evasion. From the AIV/IBV-infected HD11 cells experiment, we found that the related genes in the IFN pathway are upregulated, while Dicer and Ago2 are downregulated in the RNAi pathway. This suggests that RNA viruses may facilitate their replication by inhibiting the RNAi pathway (Fig. 1A–D). The best way to determine whether antiviral RNAi immunity occurs is to detect the production of vsiRNA. According to our findings, both the AIV-H9N2 and IBV-QX groups exhibited detectable levels of vsiRNA with a peak at 21 nt size (Fig. 1E–I). Reviewing the research of *Kennedy EM et al.,* we also paid close attention to that the length of vsiRNA produced by influenza A virus infecting DCs was mainly 21 nt, which is consistent with the results of the AIV group in our manuscript (Figs 1F and 4A) [53]. For the comparison of vsiRNA analysis and antiviral research after infecting cells with the same type of virus (Influenza A virus, IAV vs AIV, and SARS-CoV-2 vs IBV), it is also some work that our research group will continue to do in the future. Besides, negative-stranded vsiRNA was predominant in the AIV group, whereas positive-strand vsiRNA was in the IBV group (Fig. 1F and H). The distribution of vsiRNA in the viral genome can verily reflect the host's ability and preference to cleave viral dsRNAs (Fig. 2A-B). Our results also indicate that vsiRNA production and silencing are mediated by the Dicer-Ago2-vsiRNA axis, which plays a crucial role in combating RNA viruses (Fig. 3E–G).

However, despite the current absence of definitive evidence indicating that positive-stranded RNA viruses predominantly produce more (+) vsiRNA and negative-stranded RNA viruses generate predominantly (-) vsiRNA, our manuscript indeed observed this phenomenon in both the IBV-infected group and the AIV-infected group. Nevertheless, further experimental validation is imperative to ascertain whether this phenomenon is consistent across other viruses or cell types. Additionally, it is plausible that the replication and translation of IBV occur within the cytosol. Since IBV does not necessitate nuclear entry and lacks a capping step, its double-stranded RNA (dsRNA) intermediates may exhibit enhanced instability within the cytosolic milieu. The precise impact of this instability on the engagement of these intermediates by Dicer remains elusive.

As shown in the study by Backes *et al.*, the length distribution of vsiRNA varies among the fibroblasts infected with different viruses. Borna disease virus group is mainly 21 nt, Influenza A virus and Sindbis virus groups are mainly 19 nt, and the Vesicular stomatitis virus group is mainly 22 nt [11]. In the research of Li *et al.*, the group of Norovirus is mainly 18 nt [54]. The length of vsiRNA that is most abundant in the vertebrate animal group has not been reported. Only the relatively high abundance of vsiRNA between 18 and 25 nt can now be established. The large-scale analysis of vsiRNA based on their antiviral efficacy is significant for broad-spectrum antiviral therapy. Interestingly, vsiRNA also can be found in the NDV, IBDV, BTV, and SARS-CoV-2 groups with a higher abundance at the 5′ and 3′ terminus, not BVDV and BRSV groups (Fig. 4 and Supplementary Figs S7 and S8). As for whether other animal viruses will produce vsiRNA after infecting cells or animal tissues, it is still a mystery that needs further research to explore. For example, vsiRNA was not detected in the positive ssRNA bovine viral diarrhea virus (BVDV) dataset but was detected in the severe acute respiratory syndrome coronavirus type 2 dataset. Could this difference be due to the interaction between the virus and host RNAi mechanisms, potential virus inhibition mechanisms, RNA modifications, and differences in cell type specific responses. As we all know, Dicer can process Pre-miRNA and dsRNA into miRNA and siRNA. A conserved GYM motif involved in miRNA detection and cleavage was discovered in recent studies [55, 56]. Our result also found the RWM motif in vsiRNA, a paired purine A or G (R), a mismatched A or less favorably U (W), and a paired A or U (M) at positions -1, 0, and 1, respectively (Fig. 5). Besides, the plaque test result showed that double-stranded vsiRNA that maximally conforms to the RWM motif has better antiviral effects, indirectly indicating that Dicer prefers cutting vsiRNA that conforms to the RWM motif (Fig. 5F and G).

It is well known that one or more Dicer proteins are responsible for producing small RNA in eukaryotes [50, 56]. Some studies indicated that a novel Dicer isoform in mammalian stem cells (AviD) and oocytes (DicerO) functions in viral defense [36, 37, 57]. Invigoratingly, we also found that birds might also possess a Dicer isoform (DicerM) which lacks exon 9 and exon 10. Dicer and DicerM play a critical role in inhibiting RNA virus replication (Fig. 6). At the same time, previous studies in mammals have revealed that the Hel domain of AviD is closer to the dsRNA recognition receptors RIG-I, MDA5, and LGP2 than Dicer, indicating the stronger antiviral ability of AviD in mammals than Dicer [36, 38, 58, 59]. Dicer and DicerM executed their antiviral function mainly by recognizing and slicing dsRNA of RNA viruses. Structure analysis of the Hel domain revealed that Gallus-DicerM was more similar to Homo sapiens RIG-I than Gallus-Dicer (Fig. 6K and Supplementary Tables S5 and S6). Another confusing point is that previous studies showed that mammals use LGP2 protein to bind Dicer and regulate their RNAi, indicating a mutually inhibitory relationship between the RNAi and IFN systems in mammals [9, 39]. On the contrary, we wondered why RNAi

performs better in bird. Our molecular docking, western blotting, and CO-IP results showed that the RNAi system (DicerM and Dicer) and IFN system (LGP2 and MDA5) have a collaborative antiviral relationship, and both RNAi and IFN play an important role in reducing the load of RNA viruses in bird (Fig. 7 and Supplementary Figs S11–S13). For the vsiRNA application, based on GWM motif screening, we conducted antiviral plasmid using AIV and IBDV vsiRNA region (Fig. 8A). In conclusion, the vsiRNA-based prevention and control strategy using PS-vsiRNA plasmid in conjunction with PEI worked well (Fig. 8F–H).

Conclusion

RNAi is a highly conserved gene silencing mechanism that functions quickly, efficiently, and precisely in antiviral processes. Our findings show that RNA virus infection in chicken cells can detect a certain level of vsiRNA and cause the RNAi phenomenon. The vsiRNA that has been screened using the RWM motif can be made into PS-vsiRNA plasmids and joint the nanomaterial PEI to the PPvPNs that used to create therapeutic vaccinations. Our research provides a crucial theoretical foundation for the management and prevention of different RNA viruses in bird.

Acknowledgements

We are very grateful to Professor Liao Ying (Shanghai Veterinary Research Institute, Chinese Academy of Agricultural Sciences) and Wang Zhisheng (Jiangsu Academy of Agricultural Sciences) for providing the IBV-N and IBDV-VP2 antibodies. All animal experiments were approved by the Institutional Animal Care and Use Committee of Nanjing Agricultural University and performed according to the National Institutes of Health guidelines.

Authors' contributions: Y.W. constructed the avian virus infection model and carried out the molecular genetic studies, and bio-information-related data analyses charged for Figs 1–8. P.L. and J.Z. performed research on IBV infection experiment, which is related to Figs 1 and 2. C.W., N.X., and W.J. performed an IBDV infection experiment related to Fig. 8. M.F. performed bio-information-related data analyses related to Fig. 7. Z.W. provided the IBDV viruses and the anti-VP2 antibody and help to build the avian viruses infection model, which is related to Figs 1 and 8. J.L. designed and carried out the manuscript drafting; he was also the principal investigator of the project. Q.Y. conceived the study, participated in its design, and helped to draft the manuscript.

Supplementary data

Supplementary data is available at NAR online.

Conflict of interest

The authors of this editorial have no conflicts of interest to declare. The authors have no other relevant affiliations or financial involvement in any organization or entity with a financial interest in or financial conflict with the subject matter or materials discussed in the manuscript apart from those disclosed. All authors are agreed to publish this manuscript.

Funding

This work was supported by the National Key Research and Development Program of China (2021YFD1801105), the Project of Sanya Yazhou Bay Science and Technology City (SCKJ-JYRC-2022–31), the National Natural Science Foundation of China (32072835) and the Jiangsu Excellent Youth Natural Science Foundation (BK20190077) to J.L. Moreover, this work was also supported by the National Natural Science Foundation of China (31930109), the Fundamental Research Funds for the Central Universities (KYT2023004), and A Project Funded by the Priority Academic Program Development of Jiangsu Higher Education Institutions (PAPD) to Q.Y and J.L. Funding to pay the Open Access publication charges for this article was provided by National Key Research and Development Program of China Stem Cell and Translational Research, (Grant/Award Number: 2021YFD1801105').

Data availability

The RNA sequencing data have been deposited to the NCBI GEO database (Database: GSE285054, GSE285055, GSE285056). This paper does not report original code. Any additional information required to reanalyze the data in this paper is available from the lead contact upon request.

References

1. Diamond M, Halfmann P, Maemura T *et al.* The SARS-CoV-2 B.1.1.529 Omicron virus causes attenuated infection and disease in mice and hamsters. *Res Sq* 2021;**603**:687–92. https://doi.org/10.21203/rs.3.rs-1211792/v1
2. Hu B, Guo H, Zhou P *et al.* Characteristics of SARS-CoV-2 and COVID-19. *Nat Rev Micro* 2021;**19**:141–54. https://doi.org/10.1038/s41579-020-00459-7
3. Zhu N, Zhang D, Wang W *et al.* A novel coronavirus from patients with pneumonia in China, 2019. *N Engl J Med* 2020;**382**:727–33. https://doi.org/10.1056/NEJMoa2001017
4. de Breyne S, Vindry C, Guillin O *et al.* Translational control of coronaviruses. *Nucleic Acids Res* 2020;**48**:12502–22. https://doi.org/10.1093/nar/gkaa1116
5. Hatcher EL, Zhdanov SA, Bao Y *et al.* Virus variation resource - improved response to emergent viral outbreaks. *Nucleic Acids Res* 2017;**45**:D482–90. https://doi.org/10.1093/nar/gkw1065
6. He WT, Hou X, Zhao J *et al.* Virome characterization of game animals in China reveals a spectrum of emerging pathogens. *Cell* 2022;**185**:1117–29. https://doi.org/10.1016/j.cell.2022.02.014
7. Kanda A, Ishizuka ET, Shibata A *et al.* A novel single-strand RNAi therapeutic agent targeting the (Pro)renin receptor suppresses ocular inflammation. *Mol Ther Nucleic Acids* 2017;**7**:116–26. https://doi.org/10.1016/j.omtn.2017.01.001
8. Berkhout B. RNAi-mediated antiviral immunity in mammals. *Curr Opin Virol* 2018;**32**:9–14. https://doi.org/10.1016/j.coviro.2018.07.008
9. van der Veen AG, Maillard PV, Schmidt JM *et al.* The RIG-I-like receptor LGP2 inhibits dicer-dependent processing of long double-stranded RNA and blocks RNA interference in mammalian cells. *EMBO J* 2018;**37**:e97479. https://doi.org/10.15252/embj.201797479
10. Ivashkiv LB. IFNgamma: signalling, epigenetics and roles in immunity, metabolism, disease and cancer immunotherapy. *Nat Rev Immunol* 2018;**18**:545–58. https://doi.org/10.1038/s41577-018-0029-z
11. Backes S, Langlois RA, Schmid S *et al.* The Mammalian response to virus infection is independent of small RNA silencing. *Cell Rep* 2014;**8**:114–25. https://doi.org/10.1016/j.celrep.2014.05.038

12. Zhao Y, Cheng JL, Liu XY *et al.* Safety and efficacy of an attenuated Chinese QX-like infectious bronchitis virus strain as a candidate vaccine. *Vet Microbiol* 2015;**180**:49–58. https://doi.org/10.1016/j.vetmic.2015.07.036
13. Liniger M, Summerfield A, Zimmer G *et al.* Chicken cells sense influenza A virus infection through MDA5 and CARDIF signaling involving LGP2. *J Virol* 2012;**86**:705–17. https://doi.org/10.1128/JVI.00742-11
14. Elbashir SM, Lendeckel W, Tuschl T. RNA interference is mediated by 21- and 22-nucleotide RNAs. *Genes Dev* 2001;**15**:188–200. https://doi.org/10.1101/gad.862301
15. Bogerd HP, Skalsky RL, Kennedy EM *et al.* Replication of many human viruses is refractory to inhibition by endogenous cellular microRNAs. *J Virol* 2014;**88**:8065–76. https://doi.org/10.1128/JVI.00985-14
16. Guo Z, Li Y, Ding SW. Small RNA-based antimicrobial immunity. *Nat Rev Immunol* 2019;**19**:31–44. https://doi.org/10.1038/s41577-018-0071-x
17. Hoehener C, Hug I, Nowacki M. Dicer-like enzymes with sequence cleavage preferences. *Cell* 2018;**173**:234–47. https://doi.org/10.1016/j.cell.2018.02.029
18. Jinek M, Doudna JA. A three-dimensional view of the molecular machinery of RNA interference. *Nature* 2009;**457**:405–12. https://doi.org/10.1038/nature07755
19. Echebli N, Tchitchek N, Dupuy S *et al.* Stage-specific IFN-induced and IFN gene expression reveal convergence of type I and type II IFN and highlight their role in both acute and chronic stage of pathogenic SIV infection. *PLoS One* 2018;**13**:e0190334. https://doi.org/10.1371/journal.pone.0190334
20. Kakumani PK, Ponia SS, RK S *et al.* Role of RNA interference (RNAi) in dengue virus replication and identification of NS4B as an RNAi suppressor. *J Virol* 2013;**87**:8870–83. https://doi.org/10.1128/JVI.02774-12
21. Mukhopadhyay U, Chanda S, Patra U *et al.* Biphasic regulation of RNA interference during rotavirus infection by modulation of Argonaute2. *Cell Microbiol* 2019;**21**:e13101. https://doi.org/10.1111/cmi.13101
22. Wu Y, Li Y, Zhao J *et al.* IBV QX affects the antigen presentation function of BMDCs through nonstructural protein16. *Poult Sci* 2023;**102**:102620. https://doi.org/10.1016/j.psj.2023.102620
23. Sun X, Wang Z, Shao C *et al.* Analysis of chicken macrophage functions and gene expressions following infectious bronchitis virus M41 infection. *Vet Res* 2021;**52**:14. https://doi.org/10.1186/s13567-021-00896-z
24. Qi X, Liu C, Li R *et al.* Modulation of the innate immune-related genes expression in H9N2 avian influenza virus-infected chicken macrophage-like cells (HD11) in response to Escherichia coli LPS stimulation. *Res Vet Sci* 2017;**111**:36–42. https://doi.org/10.1016/j.rvsc.2016.11.008
25. Li Y, Basavappa M, Lu J *et al.* Induction and suppression of antiviral RNA interference by influenza A virus in mammalian cells. *Nat Microbiol* 2016;**2**:16250. https://doi.org/10.1038/nmicrobiol.2016.250
26. Kong J, Bie Y, Ji W *et al.* Alphavirus infection triggers antiviral RNAi immunity in mammals. *Cell Rep* 2023;**42**:112441. https://doi.org/10.1016/j.celrep.2023.112441
27. Rao DD, Vorhies JS, Senzer N *et al.* siRNA vs. shRNA: similarities and differences. *Adv Drug Deliv Rev* 2009;**61**:746–59. https://doi.org/10.1016/j.addr.2009.04.004
28. Concordet JP, Haeussler M. CRISPOR: intuitive guide selection for CRISPR/Cas9 genome editing experiments and screens. *Nucleic Acids Res* 2018;**46**:W242–5. https://doi.org/10.1093/nar/gky354
29. Maillard PV, Ciaudo C, Marchais A *et al.* Antiviral RNA interference in mammalian cells. *Science* 2013;**342**:235–8. https://doi.org/10.1126/science.1241930
30. Aliyari R, Wu Q, Li H-W *et al.* Mechanism of induction and suppression of antiviral immunity directed by virus-derived small RNAs in drosophila. *Cell Host Microbe* 2008;**4**:387–97. https://doi.org/10.1016/j.chom.2008.09.001
31. Parameswaran P, Sklan E, Wilkins C *et al.* Six RNA viruses and forty-one hosts: viral small RNAs and modulation of small RNA repertoires in vertebrate and invertebrate systems. *PLoS Pathog* 2010;**6**:e1000764. https://doi.org/10.1371/journal.ppat.1000764
32. Xu YP, Qiu Y, Zhang B *et al.* Zika virus infection induces RNAi-mediated antiviral immunity in human neural progenitors and brain organoids. *Cell Res* 2019;**29**:265–73. https://doi.org/10.1038/s41422-019-0152-9
33. Weng KF, Hung CT, Hsieh PT *et al.* A cytoplasmic RNA virus generates functional viral small RNAs and regulates viral IRES activity in mammalian cells. *Nucleic Acids Res* 2014;**42**:12789–805. https://doi.org/10.1093/nar/gku952
34. Lee YY, Lee H, Kim H *et al.* Structure of the human DICER-pre-miRNA complex in a dicing state. *Nature* 2023;**615**:331–8. https://doi.org/10.1038/s41586-023-05723-3
35. Lee YY, Kim H, Kim VN. Sequence determinant of small RNA production by DICER. *Nature* 2023;**615**:323–30. https://doi.org/10.1038/s41586-023-05722-4
36. Poirier EZ, Buck MD, Chakravarty P *et al.t al.* An isoform of Dicer protects mammalian stem cells against multiple RNA viruses. *Science* 2021;**373**:231–6. https://doi.org/10.1126/science.abg2264.
37. Flemr M, Malik R, Franke V *et al.* A retrotransposon-driven dicer isoform directs endogenous small interfering RNA production in mouse oocytes. *Cell* 2013;**155**:807–16. https://doi.org/10.1016/j.cell.2013.10.001
38. Baldaccini M, Pfeffer S. Untangling the roles of RNA helicases in antiviral innate immunity. *PLoS Pathog* 2021;**17**:e1010072. https://doi.org/10.1371/journal.ppat.1010072
39. Zhang Y, Xu Y, Dai Y *et al.* Efficient dicer processing of virus-derived double-stranded RNAs and its modulation by RIG-I-like receptor LGP2. *PLoS Pathog* 2021;**17**:e1009790. https://doi.org/10.1371/journal.ppat.1009790
40. Aqil M, Naqvi AR, Bano AS *et al.* The HIV-1 Nef protein binds argonaute-2 and functions as a viral suppressor of RNA interference. *PLoS One* 2013;**8**:e74472. https://doi.org/10.1371/journal.pone.0074472
41. Luo QJ, Zhang J, Li P *et al.* RNA structure probing reveals the structural basis of dicer binding and cleavage. *Nat Commun* 2021;**12**:3397. https://doi.org/10.1038/s41467-021-23607-w
42. Wang J, Li Y. Current advances in antiviral RNA interference in mammals. *FEBS J* 2024;**291**:208–16. https://doi.org/10.1111/febs.16728
43. Adiliaghdam F, Basavappa M, Saunders TL *et al.* A requirement for Argonaute 4 in mammalian antiviral defense. *Cell Rep* 2020;**30**:1690–701. https://doi.org/10.1016/j.celrep.2020.01.021
44. Ali PS, John J, Selvaraj M *et al.* Nodamura virus B2 amino terminal domain sensitivity to small interfering RNA. *Microbiol Immunol* 2015;**59**:299–304. https://doi.org/10.1111/1348-0421.12253
45. Qiu Y, Xu Y, Zhang Y *et al.* Human virus-derived small RNAs can confer antiviral immunity in mammals. *Immunity* 2017;**46**:992–1004. https://doi.org/10.1016/j.immuni.2017.05.006
46. Bucher E, Hemmes H, de Haan P *et al.* The influenza A virus NS1 protein binds small interfering RNAs and suppresses RNA silencing in plants. *J Gen Virol* 2004;**85**:983–91. https://doi.org/10.1099/vir.0.19734-0
47. Zheng Y, Deng J, Han L *et al.* SARS-CoV-2 NSP5 and N protein counteract the RIG-I signaling pathway by suppressing the formation of stress granules. *Sig Transduct Target Ther* 2022;**7**:22. https://doi.org/10.1038/s41392-022-00878-3
48. Sick C, Schultz U, Staeheli P. A family of genes coding for two serologically distinct chicken interferons. *J Biol Chem* 1996;**271**:7635–9. https://doi.org/10.1074/jbc.271.13.7635
49. Qiu Y, Xu YP, Wang M *et al.* Flavivirus induces and antagonizes antiviral RNA interference in both mammals and mosquitoes. *Sci Adv* 2020;**6**:eaax7989. https://doi.org/10.1126/sciadv.aax7989
50. Samuel GH, Pohlenz T, Dong Y *et al.* RNA interference is essential to modulating the pathogenesis of mosquito-borne viruses in the yellow fever mosquito Aedes aegypti. *Proc Natl Acad Sci USA*

2023;**120**:e2213701120. https://doi.org/10.1073/pnas.2213701120
51. Wang B, Fu M, Liu Y *et al.* gga-miR-155 enhances type I interferon expression and suppresses infectious Burse disease virus replication via targeting SOCS1 and TANK. *Front Cell Infect Microbiol* 2018;**8**:55. https://doi.org/10.3389/fcimb.2018.00055
52. Yang J, Huang X, Liu Y *et al.* Analysis of the microRNA expression profiles of chicken dendritic cells in response to H9N2 avian influenza virus infection. *Vet Res* 2020;**51**:132. https://doi.org/10.1186/s13567-020-00856-z
53. Kennedy EM, Whisnant AW, Kornepati AV *et al.* Production of functional small interfering RNAs by an amino-terminal deletion mutant of human Dicer. *Proc Natl Acad Sci USA* 2015;**112**:E6945–6954. https://doi.org/10.1073/pnas.1513421112
54. Li Y, Lu J, Han Y *et al.* RNA interference functions as an antiviral immunity mechanism in mammals. *Science* 2013;**342**:231–4. https://doi.org/10.1126/science.1241911
55. Liu Z, Wang J, Cheng H *et al.* Cryo-EM structure of Human dicer and its complexes with a pre-miRNA substrate [published correction appears in Cell. *Cell* 2018;**173**:1191–203. https://doi.org/10.1016/j.cell.2018.03.080
56. Yamaguchi S, Naganuma M, Nishizawa T *et al.* Structure of the Dicer-2-R2D2 heterodimer bound to a small RNA duplex. *Nature* 2022;**607**:393–8. https://doi.org/10.1038/s41586-022-04790-2
57. Wu X, Dao Thi VL, Huang Y *et al.* Intrinsic immunity shapes viral resistance of stem cells. *Cell* 2018;**172**:423–38. https://doi.org/10.1016/j.cell.2017.11.018
58. Ahmad S, Hur S. Helicases in antiviral immunity: dual properties as sensors and effectors. *Trends Biochem Sci* 2015;**40**:576–85. https://doi.org/10.1016/j.tibs.2015.08.001
59. Langmead B, Schatz MC, Lin J *et al.* Searching for SNPs with cloud computing. *Genome Biol* 2009;**10**:R134. https://doi.org/10.1186/gb-2009-10-11-r134

Received: September 30, 2024. **Revised:** January 30, 2025. **Editorial Decision:** January 31, 2025. **Accepted:** February 5, 2025